Polarimetric Scatterometry: A Promising Technique for Improving Ocean Surface Wind Measurements from Space

W.-Y. Tsai, S. V. Nghiem, J. N. Huddleston, M. W. Spencer, B. W. Stiles, and R. D. West

Jet Propulsion Laboratory, MS 300-319
California Institute of Technology
4800 Oak Grove Drive
Pasadena, CA 91109

Abstract —

Spaceborne wind scatterometers provide useful measurements of ocean surface winds and are important to climatological studies and operational weather forecasting. Past and currently planned scatterometers use measurements of the co-polarized backscatter cross-section at different azimuth angles to infer ocean surface wind speed and direction. Although successful, current scatterometer designs have limitations: degraded wind performance in the near-nadir and outer regions of the measurement swath, and a reliance on external wind information for vector ambiguity removal. Theoretical studies of scattering from the wind-induced ocean surface indicate that polarimetric measurements provide orthogonal and complementary directional information to aid the wind retrieval process. In this paper, potential benefits of making polarimetric backscatter measurements to improve wind retrieval performance are addressed. To investigate the performance of a polarimetric scatterometer, a modified version of the Jet Propulsion Laboratory *SeaWinds* end-to-end simulator is employed. To model the effect of realistic measurement errors, expressions for polarimetric measurement variance and bias are derived. It is shown that a polarimetric scatterometer can be realized with straightforward and inexpensive modifications to a current scanning pencil-beam scatterometer system, such as *SeaWinds*. Simulation results show that such a system can improve wind performance in the nadir region and eliminate the reliance on external wind information. The mechanism by which the addition of polarimetric measurements improves wind vector retrieval is discussed in detail. Field experiments are suggested to better characterize the polarimetric scattering properties of the ocean surface for future applications to wind scatterometry.

I. Background and Introduction

Frequent, global measurements of ocean surface vector winds are important to the study of the Earth's climate and have found increased utility in operational weather forecasting. To date, routine measurements of global ocean wind vectors from space have been carried out exclusively by scatterometers. Wind scatterometers are microwave radars which measure ocean surface backscatter cross-section (σ_o) at several different azimuth angles. Because σ_o is a sensitive function of wind speed and direction, the backscatter measurements can be used to solve for an estimate of the surface wind. The relationship between the wind vector, the radar illumination incidence angle, the illumination azimuth angle, the radar polarization, and σ_o is referred to as the geophysical model function (GMF). Past scatterometers and those planned for the near future use co-polarized measurements together with azimuth diversity to retrieve wind vectors. Though these measurements have proven to be immensely valuable to scientists and meteorologists, additional improvements in wind vector accuracy and coverage are desirable. In this paper, a polarimetric method is proposed as an extension to the traditional co-polarization technique in order to significantly improve the fidelity and utility of scatterometer wind measurements from space.

A. Conventional Wind Scatterometry

The wind scatterometer technique has been extensively validated by the flights of the Seasat-A Scatterometer (SASS), the Active Microwave Instrument (AMI) on ERS-1 and -2, and by the NASA Scatterometer (NSCAT) on the ADEOS mission [1, 10, 18]. All of these previous scatterometers have been "fan-beam" systems, so called because they employ multiple fixed antennas to cast broad fan shaped beams on the Earth's surface at the multiple azimuth angles necessary to measure wind. Although successful, fan-beam systems have exhibited two deficiencies: 1) the antennas are large and difficult to accommodate on spacecraft, and 2) due to the beam geometry employed by SASS, ERS, and NSCAT, backscatter measurements in the region $\pm$200km to either side of the nadir-track are at small incidence angles and are insensitive to wind direction, thus creating a large "nadir-gap" in the swath coverage [18, 25].

To alleviate the drawbacks inherent in the fan-beam design, NASA has developed the *SeaWinds* scatterometer which is scheduled to fly aboard the *QuikSCAT* spacecraft in May 1999, and aboard the ADEOS-2 mission in 2000. *SeaWinds* employs a one meter diameter dish antenna with center feeds slightly off-axis to generate two pencil-beams – the "inner" beam at an off-nadir angle of 40°, and the "outer" beam at an off-nadir angle of 46° (see Fig. 1(a)). The antenna is then conically scanned such that each point on the Earth within the inner 700 km of the swath is viewed from four different azimuth directions – twice by the inner beam looking forward then aft, and twice by the outer beam in a similar fashion [25] (see Fig. 1b). *SeaWinds* is considerably more compact than past fan-beam designs. Although the pencil-beam approach adopted by *SeaWinds* significantly lessens the "nadir-gap" problem by making measurements at suitably high incidence angles, the problem is not completely eliminated. Measurements in the extreme inner and outer swath still suffer some degradation because the relative azimuth angles of backscatter measurements are too close together (approaching 0° for the outer swath), or are too far apart (approaching 180° for the inner swath) to determine wind direction accurately.

In addition to varying degrees of difficulty in measuring winds near nadir, all scatterometers to date suffer from the occasional inability to choose the correct wind direction from a set of possible solutions. Simply put, such "ambiguities" in wind direction are caused by the sinusoidal relationship of σ_o to wind direction as observed in the model function – i.e., a wind blowing due North produces a similar cross-section to one blowing due South. To resolve the ambiguity in wind direction, numerical weather models have been used to provide external, a priori information to "nudge" the solution to the most likely value [5, 14]. Although variations of this technique have been demonstrated to significantly improve scatterometer wind direction performance, it is desirable to eliminate reliance on such external information to avoid biasing the instrument results to the model calculations.

B. Polarimetric Wind Scatterometry

A *polarimetric* scatterometer simultaneously measures conventional co-polarized backscatter and the polarimetric correlation of the co- and cross-polarized radar returns from the ocean surface. Based on general symmetry properties of the polarization components of the backscattered electromagnetic field from the wind-induced sea surface, it has been shown that the normal-

ized co-polarization and cross-polarization backscattering cross sections (σ_{HH}, σ_{VV}, and σ_{HV}) are symmetric with respect to the wind direction [20, 28, 30, 33], while the correlation between co-polarized and cross-polarized backscattering (σ_{hvvv} and σ_{vhhh}) are odd functions with respect to the wind direction [20, 33]. The different symmetry properties between the co-polarization and polarimetric correlation signatures can, in principle, be used to improve the ability to resolve wind direction ambiguities as well as generally enhance the overall wind retrieval performance across the measurement swath.

In this paper, we introduce the concept of a polarimetric wind scatterometer (PSCAT), simulate its performance, demonstrate its potential to improve scatterometer wind measurements, and show that the implementation of such a system can easily be achieved by a simple extension of existing conventional scatterometer hardware. In Section II, we first review the theoretical foundation and the fundamental properties of polarimetric scattering from the ocean surface. We then present the theoretical basis, the experimental evidence, and the assumptions used to develop a polarimetric model function for use in simulation and evaluation studies. In Section III, we discuss the wind retrieval process in light of a polarimetric scatterometer system. An intuitive discussion is provided to demonstrate the that these new measurements have the potential to improve wind accuracy. A "strawman" instrument concept, based on straightforward modifications of the *SeaWinds* design, is presented in Section IV. Key performance issues such as measurement variance and inter-channel cross-talk are also addressed. In Section V, we present an end-to-end simulation used for the performance evaluation of a PSCAT. Simulation results are presented in Section VI, showing that a simple extension of the SeaWinds design to incorporate polarimetric capability has potential to significantly improve wind performance across the swath without using external information. Finally, we conclude by describing plans for future study and experiments to further establish the polarimetric model function and verify the polarimetric scatterometer concept.

II. Polarimetric Signature of the Ocean Surface

In this section we define the backscatter coefficients referred to throughout this paper. The theoretical and observed behavior of the conventional co-polarized and cross-polarized backscatter, as well as the theoretical behavior of the polarimetric backscatter from the sea surface are described. Finally, a parametric formulation for a polarimetric model function, useful for investigating the potential of such measurements to improve scatterometer derived winds, is presented.

A. Polarimetric Backscattering Coefficients

For an incident electric field, $\overline{E}_i = (\hat{h}E_{hi} + \hat{v}E_{vi})$, the backscattered field, $\overline{E}_s = (\hat{h}E_{hs} + \hat{v}E_{vs})$, is defined as follows [19]

$$\begin{bmatrix} E_{hs} \\ E_{vs} \end{bmatrix} = \frac{e^{ikr}}{r} \overline{\overline{F}} \cdot \begin{bmatrix} E_{hi} \\ E_{vi} \end{bmatrix} = \frac{e^{ikr}}{r} \begin{bmatrix} f_{hh} & f_{hv} \\ f_{vh} & f_{vv} \end{bmatrix} \cdot \begin{bmatrix} E_{hi} \\ E_{vi} \end{bmatrix} \tag{1}$$

where the factor e^{ikr}/r accounts for the spherically propagating scattered wave front and the scattering matrix $\overline{\overline{F}}$ describes polarimetric backscattering characteristics of the ocean surface. The matrix element $f_{\mu\nu}$ is for scattered polarization μ and incident polarization ν, with μ and ν becoming "h" for the horizontal polarization or "v" for the vertical.

With the incident and scattered fields given in (1), the polarimetric backscattering coefficients are defined by

$$\sigma_{\mu\tau\nu\kappa} = \lim_{A,r\to\infty} \frac{4\pi r^2}{A} \frac{\langle E_{\mu s} E^*_{\nu s} \rangle}{\langle E_{\tau i} E^*_{\kappa i} \rangle} \tag{2}$$

where the subscripts μ, ν, τ, and κ can be either "h" or "v" and A is the illuminated surface area. In general, the four elements in the scattering matrix lead to a full four-by-four polarimetric covariance matrix composed of 16 scattering coefficients. In the backscattered direction, the principle of reciprocity dictates that $f_{hv} = f_{vh}$ in the incident polarization basis [19], and the backscattering covariance matrix, $\overline{\overline{C}}$, is reduced to the three-by-three hermitian matrix

$$\overline{\overline{C}} = \begin{bmatrix} \sigma_{hhhh} & \sigma_{vhhh} & \sigma_{hhvv} \\ \sigma^*_{vhhh} & \sigma_{hvhv} & \sigma_{hvvv} \\ \sigma^*_{hhvv} & \sigma^*_{hvvv} & \sigma_{vvvv} \end{bmatrix} \tag{3}$$

The diagonal elements of $\overline{\overline{C}}$ in (3) are the conventional co-polarization backscatter which are notationally shortened as $\sigma_{HH} = \sigma_{hhhh}$ and $\sigma_{VV} = \sigma_{vvvv}$, and the conventional cross-polarization backscatter, shortened as $\sigma_{HV} = \sigma_{hvhv}$. Spaceborne wind scatterometers such as SASS, the ERS AMI, NSCAT, and *SeaWinds* measure σ_{HH} and/or σ_{VV} over the ocean.

B. Ocean Backscatter Signatures

For the conventional co-polarization backscattering coefficients σ_{HH} and σ_{VV}, which have been extensively measured with airborne and spaceborne scatterometers, the azimuth modulation signature is well approximated by a second-harmonic even-function of the form [8, 22, 28, 30]

$$\sigma_{PP}(U, \phi, \theta) = A_0(U, \theta, PP) + A_1(U, \theta, PP)\cos(\phi) + A_2(U, \theta, PP)\cos(2\phi) \qquad (4)$$

where PP is "HH" for the horizontal co-polarization backscatter and "VV" for the vertical, θ is the incidence angle, U is the neutral wind speed at a given height, ϕ is the measurement azimuth angle defined with respect to upwind, and A_0, A_1, and A_2 are coefficients which are dependent on incidence angle, polarization, and wind speed.

In (4), the mean backscatter term, A_0, mainly carries the information on wind speed, A_1 describes the upwind/downwind asymmetry, and A_2 accounts for the difference in backscatter extrema (i.e., the upwind/crosswind asymmetry). Such co-polarization signatures are characterized by two significant features:

a. Reflection symmetry across the vertical plane parallel to the upwind/downwind direction because $\sigma_{PP}(\phi) = \sigma_{PP}(-\phi)$.

b. Upwind/downwind asymmetry which shifts the ocean azimuth modulation signatures away from the reflection symmetry condition across the vertical plane parallel to the crosswind direction.

Although much less empirical information exists, aircraft experiments and scattering theory indicate that the conventional cross-polarized return from the ocean surface takes a form similar to (4), with PP as "VH" or "HV" (see, for example, the sample aircraft data displayed in Fig. 2 and Ref. [33]). Although similar in functional form, the mean value of σ_{HV} is significantly smaller than the co-polarized backscatter at the same wind speed.

For the polarimetric backscattering coefficients σ_{vhhh} and σ_{hvvv}, there is, at this writing, no experimental data. Nevertheless, the azimuth modulation signatures in the polarimetric backscatter must obey the same physics that give rise to the reflection symmetry and upwind/downwind asymmetry conditions exhibited in the co-polarization signatures as presented above. The physics of polarimetric scattering from a surface where symmetry conditions apply, such as the ocean, have been examined in previous studies [19, 33]. These results constrain and dictate the general characteristics of the polarimetric backscatter signature. First, when the reflection symmetry across the vertical plane parallel to the upwind or downwind direction is applied, σ_{vhhh} and σ_{hvvv} must be functions that become zero on the symmetry plane. Therefore, the polarimetric backscatter can be represented in azimuth as an odd sinusoidal function with a zero mean. Second, the upwind and downwind asymmetry exhibited by the wind-induced ocean leads to an asymmetric shift across the vertical plane parallel to the crosswind direction. Consequently, the polarimetric backscatter will not be exactly zero at the crosswind direction unless the ocean conditions approach a situation where directional preference in not present, such as at very low or very high winds.

To satisfy both the reflection symmetry and and upwind/downwind asymmetry conditions, the polarimetric backscattering coefficients can be expressed in the following zero-mean, odd-function second-harmonic form

$$\sigma_{\mu\nu\tau\kappa}(U,\phi,\theta) = \alpha_1(U,\theta,\mu\nu\tau\kappa)\sin(\phi) + \alpha_2(U,\theta,\mu\nu\tau\kappa)\sin(2\phi) \tag{5}$$

where $\mu\nu\tau\kappa = vhhh$ or $hvvv$. Note that polarimetric backscatter has no wind speed dependent mean of bias term analogous to A_0 in (4).

It is important to note that the results of this paper are based on the assumption that the symmetry and asymmetry properties in both the conventional and the polarimetric backscattering coefficients are correct at least to first order. Although strong theoretical and empirical evidence suggest that this is the case, proof of the validity of the functional forms of the ocean azimuth signatures requires experimental measurements using combinations of surface-based, airborne, or spaceborne polarimetric scatterometer in conjunction with in-situ oceanic and atmospheric measurements.

C. Geophysical Model Functions

The geophysical model function is a quantitative relationship between the expected value of the backscatter coefficient and the wind vector, illumination incidence angle, azimuth angle, and polarization associated with the measurement. To proceed with our analysis we require both a conventional geophysical model function for the co- and cross-polarized returns (referred to as "CGMF" for this analysis), and a polarimetric model function (referred to as "PGMF"). Effectively, the model function quantifies the coefficients A_0, A_1, and A_2 in (4), and α_1 and α_2 in (5). In the following subsections, we review the the know CGMF and present a parametric estimate of the PGMF to be used for the polarimetric wind retrieval evaluation.

C.1. Co-polarization Geophysical Model Function

Even though increased understanding of the dynamics of wind-wave generation and of radar backscattering theory from realistic sea surfaces promises to allow a future construction of fully analytic model functions, all operational satellite scatterometer model functions developed to date have been empirically based. For these model functions, adjustable coefficients are determined through analyses of in situ measurements or statistics calculated from proxy data – such as surface wind velocities from operational global numerical weather prediction analyses, or spatially and temporally colocated wind speeds from in situ sensors other satellite instruments.

The development of a GMF for co-polarized backscatter has evolved over the past two decades [13, 23, 28], and there are still significant uncertainties at low and high wind conditions [2]. The SASS empirical model function was developed for the Seasat scatterometer [28, 29]. This model function was refined and re-validated for NSCAT. Wentz and Smith [30] and Freilich et al. [8] describe the approach and results leading to the NSCAT-1 empirical model function. A slight refinement of the NSCAT-1 model function, the NSCAT-2 model function, was adopted for the final reprocessing of the entire mission of NSCAT. In this paper, we shall therefore assume the NSCAT-2 model function for the simulation of all co-polarized ocean returns. Plots of the NSCAT-2 model function are shown in Figures 3a and 3b, for horizontal and vertical co-polarizations respectively. It follows the functional form of (4), and is an even function of the azimuth angle ϕ.

C.2. Cross-polarization geophysical model function

For the conventional cross-polarization backscattering coefficient σ_{HV}, no model function has been formally constructed due to the sparsity of experimental data. Simultaneous backscattering coefficients σ_{HV} and σ_{VV} were measured by the NUSCAT scatterometer during the Surface Wave Dynamics Experiment (SWADE) in 1991 [21, 22]. Figure 2 shows σ_{HV} (denoted by VH in the plots) and σ_{VV} at 40° and 50° incidence angles acquired by NUSCAT aboard the NASA C-130 aircraft. As derived from in-situ buoy data, neutral wind at 19.5-m height varied from the low wind speed range of 2.9-3.5 m/s at buoy A to the moderate wind range of 8.7-9.4 m/s at buoy C during the NUSCAT measurement time. NUSCAT results indicate that the cross-polarization ratio $e_V = \sigma_{HV}/\sigma_{VV}$ is around -15 dB. This result is consistent with those reported for earlier aircraft and spaceborne experiments [17].

Because they contain essentially the same directional information but at a much lower signal-to-noise ratio, measurements of conventional cross-polarized backscatter coefficients (σ_{VH} and σ_{HV}) are *not* considered as a means to retrieve the wind. Thus, in some sense, the present analysis is insensitive to the precise form of the cross-polarized model function. Some estimate of the values of these terms are required, however, in order to quantify the variance inherent in the the fully polarimetric measurements due to signal-to-noise considerations in the correlation of the co- and cross-polarized returns (see Section IV). For this purpose, in the simulation described in Sections V and VI, we shall use $e_V = -15$ dB at all wind speeds when evaluating the performance of the polarimetric scatterometer. As a sensitivity analysis, we will also evaluate the performance impact of using the conservative value of $e_V = -20$ dB as well.

C.3. Polarimetric geophysical model function

Even though no K_u-band scatterometer measurement of the polarimetric backscattering coefficients σ_{hvvv} or σ_{vhhh} has ever been conducted, a theoretical polarimetric scattering model was presented in [33] which incorporates both the relevant physics and a consideration of conventional backscatter measurements and polarimetric radiometer measurements over the ocean. This model is used to calculate σ_{hvvv} and σ_{vhhh} as a function of azimuth angle for moderate wind conditions (11.5 m/s), where the magnitude of the polarimetric coefficients is expected to be the largest.

The results indicate that the corresponding polarimetric correlation coefficients σ_{hvvv} and σ_{vhhh} are well approximated by a functional form such as (5).

In order to be useful in wind retrieval performance studies, the moderate wind results in [33] must be expanded to yield a PGMF for a range of wind speeds. For this, the following simple approach is employed. To extend the polarimetric azimuth modulation signature to low and higher wind cases, we consider the azimuth signature asymmetry determined by NSCAT-2 model function. The azimuth modulation is caused by the anisotropic directional features associated with the wind driven ocean surface. At low winds, the directional features are weak and the ocean surface approaches the isotropic condition under which the azimuth modulation in the polarimetric backscatter is weak, so we expect σ_{hvvv} and σ_{vhhh} to approach zero for all azimuth angles. At the other extreme, where the wind speed is so high that the ocean surface becomes very turbulent with breaking waves and foam, a more random scattering mechanism develops. Such random scattering at very high winds approaches a statistically isotropic condition, rendering a small value for σ_{hvvv} and σ_{vhhh} again. At a certain intermediate wind condition, the wind driven directional features on the ocean surface become most dominant and the surface anisotropy becomes strongest. We therefore choose the amplitude of the co-polarized azimuth modulations given by the NSCAT-2 GMF at different wind speed and incidence angles as anisotropy factors to scale the moderate wind results to other wind conditions. Appendix A describes the algorithm for generating the PGMF in some detail.

In Fig.s 3(c) and 3(d), the resulting PGMF for σ_{hvvv} and σ_{vhhh} for a range of wind speeds is displayed. It is important to point out that, with our current understanding of polarimetric scattering, this only represents "reasonable guess" to the true PGMF. Unlike the thoroughly studied CGMF which is assumed known for the purposes of this study, we must consider the values of α_1 and α_2 embodied by the PGMF as parametric variables. Later in this analysis when the potential wind performance of a polarimetric scatterometer is investigated by simulation, the effect of varying magnitude for the assumed polarimetric coefficients will be evaluated.

III. Wind Retrieval and Ambiguity Removal

In the previous section, both the CGMF and the PGMF for Ku-band backscatter were discussed. The process of inverting the model function to obtain a small number of possible wind vector solutions for a given set of measurements is known as *wind retrieval.* The process of selecting a single vector from the set of possible wind solutions is termed *ambiguity removal.* In this section we briefly describe the wind retrieval process, introduce the concept of solution curves, and show, via a simple example, the potential advantage of combining polarimetric measurements with co-polarized measurements.

A. Wind Retrieval Algorithm

To perform wind retrieval, we start with a set of measurements made over a specific resolution cell, called a wind vector cell (WVC), on the ocean surface. In the case of *SeaWinds*, there are typically about 50 co-polarized σ_0 measurements within a 25 x 25 km WVC [26]. The goal of wind retrieval is to use these measurements to determine the most likely wind speed and direction. Typically, this is done using a maximum likelihood estimator based on following objective function [18]:

$$J(|U_{trial}|, \phi_{trial}) = \sum_{i=1}^{N} \left(\frac{\sigma_{meas}(i) - \sigma_{trial}(i)}{\delta_{trial}(i)} \right)^2 + \ln \left(\delta_{trial}(i)^2 \right) \tag{6}$$

where $|U_{trial}|$ is the trial wind speed, ϕ_{trial} is the trial wind direction (clockwise from North), $\sigma_{meas}(i)$ is the value of the measured backscatter coefficient, $\sigma_{trial}(i)$ is the value of the trial backscattered coefficient based on the trial wind vector, and $\delta_{trial}(i)$ is the estimated variance on a measurement of the trial wind vector. The trial coefficient is determined via the model function

$$\sigma_{trial}(i) = \mathrm{GMF}\left(|U_{trial}|, \chi_{trial}, K_{meas}, \theta_{meas}\right) \tag{7}$$

where GMF is the geophysical model function, χ_{trial} is the trial wind direction relative to the measurement azimuth angle, K_{meas} is the measurement coefficient type (i.e., HH, VV, *hvvv*, or *vhhh*), and θ_{meas} is the incidence angle of the measurement.

The wind retrieval algorithm searches through trial wind speeds and relative wind directions to find a wind vector that maximizes the objective function. In general, there are several local maxima in the objective function surface, all with similar likelihoods. The wind vectors corresponding to these local maxima are retained as possible wind vector solutions, called ambiguities. The ambiguity removal process, which typically imposes a continuity constraint or utilizes median filtering on the field, is then applied to yield one "selected" vector [14, 18, 24].

B. Single Beam and Two Beam Solution Curves

To intuitively visualize the wind retrieval process, let us first consider the outer beam of the *SeaWinds* scatterometer. This beam is vertically polarized and has a look angle of 46° producing measurements of the ocean's surface with an incidence angle of 54°. As the antenna rotates, the outer beam will make measurements along a 900 km radius scan (see Fig 1(a)). Fig. 1(b) shows a specific target on the ocean being viewed twice by the outer beam: once when the spacecraft is at position 1 and again after the spacecraft has moved to position 4. Assuming the wind over the target has a speed of 7 m/s and a direction of 30°, in Fig. 4(a) we plot a *solution curve* for each of the two σ_0 measurements made by the outer beam. A solution curve is a curve showing the wind speed that maximizes the objective function (6) for each relative wind direction. Note that the variance term is effectively discarded when computing the objective function for a single measurement and so the solution curves shown do not indicate the relative weight of measurements in the objective function. The most likely wind vectors are at the intersections of the solution curves, and have been indicated by circles. We see that the two solution curves intersect in four places, producing four ambiguities. These four ambiguities have similar likelihoods, and additional information is needed to aid in the selection of a single ambiguity to represent the retrieved wind.

Scatterometers typically make multiple measurements having different polarizations, incidence angles, and/or azimuth angles in order to help select a single wind vector solution. Changes in polarization and incidence angle tend to have a small effect on the shapes of solutions curves. Making measurements at a different azimuth angle is the most effective technique (for conventional scatterometry) because it produces a phase shift in the solution curves thus causing their intersections to be better defined, especially in the presence of noise. This is the primary technique employed by the *SeaWinds* scatterometer which uses a second beam, the inner beam, with

a smaller look angle to obtain additional measurements at different azimuth angles [25, 26]. In Fig. 1(b) we see that the target WVC is measured by the inner beam when the spacecraft is at locations 2 and 3. *SeaWinds'* inner beam is horizontally polarized enabling it to take advantage of the slight difference in the σ_{HH} and σ_{VV} model functions. Fig. 4(b) shows the solutions curves for both the inner and outer beam. The wind vector ambiguities are indicated by circles. For this two-beam system, we note that the only place where all four solution curves perfectly intersect is at the true wind speed and direction (7 m/s at 30°).

In reality, each σ_0 measurement is noisy (cf. Section V) and this can be approximated by shifting its solution curve up or down. How much a solution curve shifts depends on the magnitude of the error in σ_0 and on the relationship between σ_0 and wind speed. In Fig. 4 (b) we note that if we shifted the higher of the co-polarized solution curves (dotted line) upward, it would no longer intersect the other solution curves at the true wind vector and would start to form a better intersection with the other curves near 70°. For the *SeaWinds* instrument, we find that the errors in σ_0 are sufficiently large that we can not rely solely on the instrument for the selection of ambiguities and we require an additional external data source to aid the ambiguity removal process. The technique of allowing the ambiguity removal process to be loosely constrained by a numerical model field has been termed "nudging," and has been utilized in various forms by both NSCAT and the ERS AMI [5, 14].

C. Polarimetric Scatterometer Wind Retrieval

Let us now examine the potential performance of the above example when polarimetric capability is added: in addition to the co-polarized measurements we add σ_{hvvv} measurements on the outer beam and σ_{vhhh} measurements on the inner beam. The geometry for these additional measurements will be the same as the geometry for the co-polarized measurements. We can achieve polarimetric capability with minor modifications to the *SeaWinds* hardware as discussed in Section IV. An advantage of this approach is that the *hvvv* measurements can be made simultaneously with the VV measurements and the *vhhh* measurements can be made simultaneously with the HH measurement without needing to sacrifice transmit power or integration time, as would be the case with additional co-polarized measurements.

Fig. 4 (c) shows the solution curves for the *hvvv* and *vhhh* measurements, assuming the

polarimetric model function formulated in Section II, together with the traditional co-polarized measurements. As expected, we see that the only place where all of the solution curves intersect is at the true wind vector solution. What is significant here is that the *hvvv* and *vhhh* solution curves do not pass close to the incorrect co-polarized ambiguities. The correlation measurements strongly support the correct solution and provide little support for the undesired ambiguities. We also note that the solution curves for the *hvvv* and *vhhh* measurements are dramatically different in character from the solution curves for the co-polarized measurements. The polarimetric curves only cover portions of the azimuth space, extend up to higher wind speeds, and tend to have much higher slope than the co-polarized solution curves. This behavior is due to the zero mean nature of the PGMF.

In this section, we have shown that the addition of *hvvv* and *vhhh* measurements shows promise for improving ambiguity removal performance. Since these measurements also provide additional information, we anticipate that they will improve the retrieved wind vector accuracy as well. To obtain a more quantitative assessment of performance improvements, we next develop a instrument design and noise model, and conduct an end-to-end polarimetric scatterometer performance simulation.

IV. Polarimetric Scatterometer Instrument Description

In this section, a realizable polarimetric instrument concept is presented. Several implementations are possible, but here we are most interested in developing a sample instrument model that can be used in performance simulations to evaluate the potential of the polarimetric scatterometer technique. The concept adopted is based on the *SeaWinds* instrument [25, 26] with straightforward modifications to enable the simultaneous reception of both the co-polarized and cross-polarized returns. Several important signal processing issues, unique to polarimetric scatterometry, are then addressed. Included in this discussion is a derivation of the measurement variance for the polarimetric backscatter coefficients (σ_{hvvv} and σ_{vhhh}), which is a key factor in determining the wind measurement performance.

A. *SeaWinds* System Architecture and Measurement Geometry

A polarimetric scatterometer can be easily constructed by adding cross-polarization measurement capability to an existing pencil-beam scatterometer design such as *SeaWinds*. A brief description of the current *SeaWinds* instrument is provided here for ease of reference.

As discussed in Section I, the *SeaWinds* architecture employs a one meter diameter dish antenna with center feeds slightly scanned to generate two pencil-beams. The transmitter alternatively pulses the inner beam then the outer beam yielding an effective PRF for each beam of 92 Hz. This sampling rate, coupled with the antenna rotation rate of 18 rpm, produces measurements on the surface at 15 to 20 km spacing (see [25]).

Figure 5 (a) depicts the basic design of the *SeaWinds* radar electronics. Upon command from the timing controller, the transmitter, which consists of a modulated signal generator driving a traveling wave tube amplifier (TWTA), issues a 1.5 ms duration, 110 Watt Ku-band pulse. The pulse is routed to either the inner or the outer beam and through a coaxial rotary joint to the spinning section of the antenna assembly. The echo return is likewise directed to the receiver where it is amplified, downconverted, and detected. Due to the motion of the satellite relative to the Earth, a Doppler shift of between ± 500 kHz is imparted to the echo return signal as the antenna scans. To compensate for this effect and insure that the echo return is centered in the receiver bandwidth, a carrier offset frequency is computed as a function of the antenna azimuth and imparted to the transmit pulse. An important feature of any scatterometer system is the accurate calibration of the transmit power and receiver gain. In the *SeaWinds* instrument design, these parameters are measured simultaneously by periodically injecting the transmit pulse, attenuated by a known amount, into the receiver. A summary list of the key radar parameters is shown in Table 1.

B. Polarimetric Modifications

Because *SeaWinds* has proven easily accommodated on spacecraft, we constrain our polarimetric design to be a simple modification to this existing system. The necessary modifications to the *SeaWinds* design to add polarimetric capability are summarized in Fig.5(b). In the antenna assembly, the feed system must be modified in order to allow the simultaneous reception of the

two polarizations. This is done by employing dual-polarized feeds and orthomode transducers to separate the V and H components. The antenna design must also be modified to produce a very low cross-polarized component in order to minimize cross-talk between the channels. Preliminary design studies have demonstrated that cross-polarization isolation levels of better than 35 dB can be achieved with an offset-fed antenna/feed configuration.

To handle the more complicated switching required for the polarimetric measurements, additional circulators and/or ferrite switches are necessary on both sides of the antenna rotary joint. The switching configuration shown in Fig.5(b) is one (but by no means the only) strategy for routing the signals to insure that the co-polarized and cross-polarized returns are received simultaneously on each beam in turn. One advantage of the approach shown is that the RF connect across the rotary joint only requires two channels, just as in the current *SeaWinds* design.

The final modification is the addition of another receiver chain in order to obtain the polarimetric correlation measurements. As shown in Fig.5(b), the conventional co-polarized measurements (σ_{VV} or σ_{HH}) are obtained by detecting the total signal power out of one of the receivers by forming $\langle R_1 R_1^* \rangle$ or $\langle R_2 R_2^* \rangle$, where $R_i(t)$ is the downconverted return signal in the ith channel. The polarimetric correlation components are derived from a measurement of $\langle R_1 R_2^* \rangle$. It is important to note that all the required modifications to implement polarimetric capability involve the use of fully mature technologies, and thus do not significantly increase the cost of the system.

C. Backscatter Estimation and Measurement Variance

Noise and other error sources in the measurement of the polarimetric backscatter cross-section will translate directly into errors in wind retrieval. The performance of spaceborne scatterometer systems is fundamentally limited by the measurement variance due to radar fading and the presence of thermal noise [25]. Due to the much smaller signal strength in the cross-polarized return relative to the co-polarized return, the analysis of polarimetric measurement variance assumes further significance. Likewise due to the low cross-polarized return power, polarimetric measurements are more susceptible to channel cross-talk contamination. In order to address these important polarimetric measurement accuracy issues, we first construct a signal model which incorporates the relevant echo statistics. This model is then applied to develop expressions useful in quantifying σ_o measurement accuracy.

The downconverted signal amplitude received in the H-pol and V-pol channels, $\mathcal{A}_H$ and $\mathcal{A}_V$, at time t from a single scatterer located at position $\bar{r}$ can be represented by

$$\begin{bmatrix} \mathcal{A}_H(t,\bar{r}) \\ \mathcal{A}_V(t,\bar{r}) \end{bmatrix} = \frac{\lambda}{(4\pi)^{3/2}|\bar{r}|^2} \left\{ \begin{bmatrix} K^r_{hh}(\bar{r}) & K^r_{hv}(\bar{r}) \\ K^r_{vh}(\bar{r}) & K^r_{vv}(\bar{r}) \end{bmatrix} \cdot \begin{bmatrix} S_{hh}(\bar{r}) & S_{hv}(\bar{r}) \\ S_{vh}(\bar{r}) & S_{vv}(\bar{r}) \end{bmatrix} \cdot \begin{bmatrix} K^t_{hh}(\bar{r}) & K^t_{hv}(\bar{r}) \\ K^t_{vh}(\bar{r}) & K^t_{vv}(\bar{r}) \end{bmatrix} \cdot \begin{bmatrix} \mathcal{A}^t_H(t - \frac{2|\bar{r}|}{c}) e^{i\omega_d(\bar{r})t} \\ \mathcal{A}^t_V(t - \frac{2|\bar{r}|}{c}) e^{i\omega_d(\bar{r})t} \end{bmatrix} \right\}. \quad (8)$$

Here, $\mathcal{A}^t_H$ and $\mathcal{A}^t_V$ are the transmit signals generated for the H- and V-pol channels, which are delayed by the round-trip flight time to the scattering element $(2|\bar{r}|/c)$ and shifted in frequency by the Doppler shift of the element ω_d. The K^t's and K^r's are the amplitude gains for transmission and reception through the radar system. In general, the K^t's and K^r's are complex, and take into account the antenna pattern, RF component gains and losses, phase shifts, and all cross-talk between the two channels. Under reciprocity conditions, $K_{hv} = K_{vh}$ in both the transmit and receive gain matrices. The S's are complex random variables and form a surface scatterer matrix (not to be confused with the *scattering* matrix in Eq.(1)) defined such that

$$\langle S_{\mu\tau}(\bar{r}) S^*_{\nu\kappa}(\bar{r}') \rangle = \sigma_{\mu\tau\nu\kappa} \delta(\bar{r} - \bar{r}'). \quad (9)$$

The total signal received in each channel, C, is the combination of echo returns from all scatters that are illuminated, plus thermal noise:

$$\begin{aligned} \mathcal{Q}_H(t) &= \int d^2\bar{r} \mathcal{A}_H(t,\bar{r}) + \nu_H(t) \\ \mathcal{Q}_V(t) &= \int d^2\bar{r} \mathcal{A}_V(t,\bar{r}) + \nu_V(t), \end{aligned} \quad (10)$$

where the integral is performed over the illuminated ocean surface and the noise components in each channel (ν_H and ν_V) may be partially correlated due to cross-talk.

Co-Polarized Measurements

The conventional scatterometer measurement involves the detection of the co-polarized normalized backscatter cross-section – σ_{VV} or σ_{HH}. This process has been described by previous authors [16, 26]. In light of the expression for the fully polarimetric system described by Eq.(8), as an example we review estimation process for σ_{VV} below.

Assuming only a V-polarized signal is generated by the transmitter, $\mathcal{A}_H^t = 0$. Because $K_{vv} \gg K_{hv}$ and $\sigma_{VV} \gg \sigma_{HV}$, it is typical to assume that all cross terms in the matrices of Eq.(8) are negligible (an assumption that we will have to re-evaluate for the polarimetric case). Also assuming that the signal and noise are uncorrelated, the total received power in the channel is

$$\langle |\mathcal{Q}_V|^2 \rangle = X\sigma_{VV} + \langle |\nu_V|^2 \rangle, \tag{11}$$

where the continuous time variable t has been dropped for notational convenience. Here, we also assume that the wind, and hence backscatter, is constant over the illuminated footprint and define the parameter X as

$$X = \frac{\lambda^2}{(4\pi)^3} \int d^2\bar{r} \frac{|K_{vv}^t|^2 |K_{vv}^r|^2}{|\bar{r}|^4}. \tag{12}$$

An estimate of σ_{VV} is thus obtained from

$$\widetilde{\sigma_{VV}} = \frac{\langle |\widetilde{\mathcal{Q}_V}|^2 \rangle - \langle |\widetilde{\nu_V}|^2 \rangle}{X}, \tag{13}$$

where the tilde indicates that an estimate is performed. Typically, an estimate of the channel noise power ($\langle |\nu_V|^2 \rangle$) is obtained by observing the noise floor at a time or in a bandwidth when the signal is not present [16].

For scatterometer performance evaluation, it is also important to know the variance of the cross-section estimate. The random fluctuations of the estimate due to fading and thermal noise will effect the accuracy of the wind retrieval. For the co-polarized return, this has been derived for several different cases by previous studies [6, 16, 26]. Assuming that the echo return has a Doppler bandwidth B_s and a pulse duration T_p, and that the time-bandwidth product of the noise-only estimate $\gg B_s T_p$, the cross-section estimate variance may be approximated as

$$\mathrm{Var}[\widetilde{\sigma_{VV}}] = \frac{\sigma_{VV}}{T_p B_s} \left(1 + \frac{2}{SNR_{VV}} + \frac{1}{SNR_{VV}^2} \right), \tag{14}$$

where the signal to noise ratio is defined as

$$SNR_{VV} = \frac{X\sigma_{VV}}{\langle |\nu_V|^2 \rangle}. \tag{15}$$

Similar results are obtained for the measurement of σ_{HH}.

Polarimetric Measurements

To obtain the polarimetric cross-section σ_{hvvv} or σ_{vhhh}, we must perform a correlation of the return from the two polarization channels. For the measurement of σ_{hvvv}, we transmit V-polarization and then correlate the co-polarized return with the H-polarized cross-pol return in the other channel:

$$\langle \mathcal{Q}_V \mathcal{Q}_H^* \rangle = X_1 \sigma_{hvvv} + X_2 \sigma_{vvvv} + \ldots + \langle \nu_V \nu_H^* \rangle \tag{16}$$

Here, the term $X_1 \sigma_{hvvv}$ contains the desired information with

$$X_1 = \frac{\lambda^2}{(4\pi)^3} \int d^2\bar{r} \frac{|K_{vv}^t|^2 K_{vv}^r K_{hh}^{r*}}{|\bar{r}|^4}. \tag{17}$$

The largest "cross-talk" term is $X_2 \sigma_{vvvv}$ with

$$X_2 = \frac{\lambda^2}{(4\pi)^3} \int d^2\bar{r} \frac{|K_{vv}^t|^2 K_{vv}^r K_{hv}^{r*}}{|\bar{r}|^4}. \tag{18}$$

The "..." represents the 14 other cross-talk terms with the appropriate X's similarly defined. Note that when the cross-terms in the gain matrices are small, the contribution of the cross-talk power terms to Eq.(8) will be small as well. The term $\langle \nu_V \nu_H^* \rangle$ represents the potential for the noise in the channels to be partially correlated due to cross-talk effects.

An unbiased estimate of σ_{hvvv} is thus obtained from

$$\widetilde{\sigma_{hvvv}} = \frac{\langle \widetilde{\mathcal{Q}_V \mathcal{Q}_H^*} \rangle - \left(X_2 \widetilde{\sigma_{vvvv}} + \ldots + \langle \widetilde{\nu_V \nu_H^*} \rangle \right)}{X_1} \tag{19}$$

Note that in order to estimate σ_{hvvv}, an estimate of both the signal and noise cross-talk powers must be obtained and subtracted from the channel correlation measurement. In the case of the noise correlation term, this is straightforwardly accomplished in a manner analogous to the co-polarized "noise-only" calibration where periodic observations of the noise floor are performed. For the signal cross-talk terms, it is most desirable to design the system so that the cross-talk gains are very small, thus making the cross-talk power negligible. If this can not be completely achieved, then the cross-talk contamination must be estimated and removed by a thorough calibration of all system gains in Eq.(8).

As an example of how strong the cross-talk terms may be, consider the case of V-Pol transmitted and incident on the surface at 54° (the incident angle for the *SeaWinds* outer beam). We

further assume that the wind is blowing at 8 m/s in a direction 45° from the illumination azimuth ($\chi = 45°$). From the baseline model functions discussed in Section II, we have that $\sigma_{vv} = 0.012$ and $\sigma_{hvvv} = 0.0012$ – indicating that the cross-section of the co-polarized return is 10 dB higher than the correlation cross-section, and creating a potential for significant contamination for the largest cross-talk term in Eq.(16). If, however, the K^r_{hv} term in (8) provides sufficient attenuation relative to the K^r_{hh} term, this cross-talk will be reduced. If $|K^r_{hv}|/|K^r_{hh}| < -15$dB for all $\bar{r}$, this corresponds to a *power* isolation between the two polarization channels of better than -30 dB, and is an achievable hardware design. This implies $|X_2|/|X_1| < -15$dB, and thus the total cross-talk contamination is 5 dB below the desired signal power. Efforts to improve the isolation will further reduce the contamination and make the system insensitive to cross-talk subtraction processes.

As in the case of the conventional co-polarized measurements, we require an expression for the variance of the polarimetric correlation term in order to correctly model measurement noise in the wind retrieval process. An expression for the measurement variance for σ_{hvvv} can be derived using stochastic signal processing techniques similar to those employed to obtain (14). Assuming that the cross-talk contamination terms are on the same order or less than the desired signal term in (16), it can be shown that

$$Var[\widetilde{\sigma_{hvvv}}] = \frac{1}{2T_pB_s}\left[\sigma^2_{hvvv} + \sigma_{vv}\sigma_{HV}\left(1+\frac{1}{SNR_{VV}}\right)\left(1+\frac{1}{SNR_{HV}}\right)\right] \tag{20}$$

where we have defined

$$SNR_{VV} = \frac{X\sigma_{VV}}{\langle|\nu_V|^2\rangle} \quad \text{and} \quad SNR_{HV} = \frac{X\sigma_{HV}}{\langle|\nu_H|^2\rangle}. \tag{21}$$

Note that the variance of the correlation term is a function of both the co- and cross-polarized SNR's. Because $SNR_{VV} \gg SNR_{HV}$, the variance will be dominated by the signal-to-noise ratio in the cross-polarized return. If we constrain our polarimetric system to be of the *SeaWinds* class (i.e., one meter antenna, 110 Watt transmitter), SNR_{HV} may be quite small, particularly at low wind speeds, and the variance of the polarimetric measurements may be quite high. The significance of this high variance on the wind retrieval will be examined in more detail in Section VI.

V. End-to-End Simulation Methodology

In order to evaluate the performance of a scanning pencil-beam scatterometer with polarimetric capability, a modified version of the JPL *SeaWinds* simulator is used [31]. The simulator requires only minor modifications in order to simulate a PSCAT system, and is described in this section.

A. End-to-End Scatterometer Simulation

An end-to-end scatterometer simulator consists of two basic components: a spacecraft/instrument simulator and a data processor (see Fig. 6). The spacecraft/instrument component simulates the "flight" of the instrument over a wind-induced ocean. During this flight, the entire measurement process is modeled, including the the addition of the correct amount of noise on the simulated telemetry from which σ_0 is to be derived. Numerical model analysis fields, which contain realistic wind features, are typical used as "truth" fields. The data processor portion of the end-to-end simulator processes the simulated scatterometer data to σ_0's, colocates the σ_0's, retrieves wind vectors, and performs ambiguity removal to yield a retrieved wind field. The accuracy of the wind retrieval is determined by comparing the input wind field with the retrieved wind field and calculating metrics such as rms speed and direction errors.

B. The SeaWinds End-to-End Simulation

The development of the *SeaWinds* simulator spans several years and was based, in part, on an earlier simulator used for NSCAT [3]. It was found that the NSCAT simulator yielded a reasonable prediction of the performance of the NSCAT instrument. The simulator models four key sources of error: model function error, communication noise, instrument calibration error, and spacecraft attitude error.

A model wind field is used to provide the wind speed and direction at the location of each σ_0 measurement. The geophysical model function described in Section II provides the radar cross-section for the indicated wind speed, relative azimuth direction, incidence angle, and polarization. In nature, the radar cross-section also depends on other variables such as sea surface temperature

and salinity. In the simulator, these error sources are modeled as gamma distributed noise in the model radar cross-section, with a normalized variance that varies with wind speed and the polarization of the incident radiation (V or H) as determined via NSCAT data analysis.

The "communication noise" is the variance in an energy measurement due to fading and thermal noise. The expected value of the co-polarized energy measurements is computed using the radar equation (11), with X as defined in (12). The thermal noise energy is,

$$\langle |\nu_{V,H}|^2 \rangle = \frac{k_b T_{sys} G_{rc}}{L} B_s T_g, \tag{22}$$

where k_b is Boltzmann's constant, T_{sys} is the system temperature, L is the system loss, T_g is the receive gate width, and G_{rc} is the net channel receiver gain. Gaussian noise is added so that the radar cross-section estimate has the variance given in (14). The noisy energy measurements are incorporated into the simulated telemetry.

Unlike the preceding error sources, the *SeaWinds* instrument calibration error and the spacecraft attitude error affect the computed σ_0 indirectly by corrupting knowledge of radar parameters used in later processing. Calibration errors occur because the instrument calibration measurements (see Section IV) are themselves noisy. Based on *SeaWinds* specifications and instrument test data we model these calibration errors as a time correlated Gaussian process with a normalized standard deviation of 0.3 dB, and a correlation time of one minute. Spacecraft attitude knowledge errors also result in errors in the retrieved σ_0 because they introduce errors in the geometry calculations performed by the ground processing system. The attitude knowledge errors are modeled according to the spacecraft specifications.

C. Simulation of a Polarimetric System

In order to use the SeaWinds simulator to simulate a polarimetric scatterometer, three important extensions are needed. First, the model function is extended to incorporate cross-polarized and polarimetric correlation measurements as described in Section II. Second, the variance of the correlation measurement is computed and applied as described in Section IV, and, similar to the co-polarization case, an estimate of the model function error for correlation measurements is applied. Third, the objective function used by the maximum likelihood estimator in wind retrieval is modified to include the variance term for correlation measurements (see section III). With these

extensions in place, the simulator and data processor can be used to evaluate the wind retrieval performance that a polarimetric system can provide.

VI. Simulation Results

In this section, we use the simulation tools described previously to compare the wind performance of conventional and polarimetric scatterometer systems. We explain how even with the relatively large variance for the polarimetric measurements, the performance of a polarimetric system can be significantly better than that of conventional systems across the entire swath. Additionally, we perform simulations to show that the performance improvement is robust to parameter changes in the estimated polarimetric geophysical model function, so long as the general form of the model function is preserved.

A. PSCAT Baseline Performance

Using a set of *European Center for Medium-range Weather Forecasting* (ECMWF) one degree resolution analysis wind fields as truth, we have simulated 5 orbits of PSCAT data, and performed wind retrieval. The simulated system incorporates the polarimetric hardware modifications outlined in Section IV, the baseline polarimetric geophysical model function described in Section II, and the variance of the polarimetric measurements discussed in Section IV. Wind retrieval is performed using the *SeaWinds* Science Data Processing algorithms, which are similar to what was used on NSCAT. The wind performance is then obtained by comparing the retrieved winds with the input (true) winds.

The root mean square (RMS) wind direction and speed errors were calculated for the selected ambiguity, and plotted as a function of cross track distance for four ranges of wind speed: 3-5.5 m/s, 5.5-7.5 m/s, 7.5-10.5 m/s and 10.5-30 m/s. The results are depicted by solid lines in Fig. 7. Note that the selected wind vectors are obtained using the backscatter measurements only, without the injection of any external information (i.e., no "nudging", see Section III).

To appreciate the wind performance improvement of a PSCAT system, we compare PSCAT

results with the simulated performance of the *SeaWinds* co-polarization only system. As described in Section III, to obtain good ambiguity selection skill and consequently good wind performance, we must use external information to aid in ambiguity removal. The nudged *SeaWinds* results are shown as the dashed lines on the plot.

The results depicted in Fig. 7 indicate that incorporating the polarimetric backscattering correlation coefficient measurements significantly improves the wind retrieval performance. The direction and speed RMS errors improve across the entire swath (especially at midswath), and the need for nudging is eliminated. Improvements in two areas contribute to these results. First, the percentage of the time (skill) that the ambiguity removal algorithm selects the ambiguity nearest to the truth is nearly 100%. Secondly, the RMS speed and direction error of the ambiguity closest to the true wind vector is also reduced. Next, we explain how the additional polarimetric measurements have such a large impact on performance despite their large variance in comparison to the co-polarization measurements.

B. Understanding the Simulation Results

In order to understand the above results, we now examine the wind retrieval processes for two representative wind vector cells (WVC): one at the midswath, and the other midway between nadir and the outer swath boundary. The first example WVC was chosen to have a low wind speed (4.7 m/s) at a location near the middle of the swath (37.5 km from the nadir track). This cell was selected because its polarimetric measurements have a large variance and yet it still exhibits significant wind performance improvement (vs. conventional scatterometry).

The best way to understand the performance is to examine the wind retrieval in a probabilistic manner. Since the purpose of wind retrieval is to find the most likely wind vector for a given set of σ_0 measurements, the most relevant probability density function (pdf) is $P(u, \phi|\{\sigma_{0i}\})$, the probability density of wind vectors given an observed set of backscatter values where σ_{0i} represents the set of all the measured conventional or polarimetric coefficients. (See Appendix B for a more detailed discussion of the underlining assumptions of this pdf.) To aid in visualizing the pdf in an intuitive manner, we compute the percentile T(u, ϕ), the integral (expressed as a percentage) of the pdf over the region in wind vector space for which the pdf value is less than $P(u, \phi|\{\sigma_{0i}\})$. In this manner, we depict regions in wind direction and speed space which correspond to certain

probability values. For example, the contour corresponding to $T = 20\%$ divides the the space of possible wind vectors into two regions: a region of greater probability density with 80% total probability, and a region of lesser probability density which is 20% probable. For any given probability threshold, there is a contour in the percentile plot that defines a region with that probability.

We shall refer to a group of co-located measurements which share the same measurement type, beam, and approximately the same azimuth as a "look set." First we shall contrast the wind retrieval characteristics of single polarimetric and co-polarization look sets, then we will examine the effect of combining information from multiple look sets. Four gray scale percentile plots are shown in Fig. 8, depicting inner beam forward look measurements with (1) one σ_{vhhh}, (2) all 18 σ_{vhhh} (3) one σ_{HH}, and (4) all 18 σ_{HH}. In each plot, the dark region enclosed by the dashed contour line is 80% probable. We first note that an individual noisy polarimetric measurement provides little information. Increasing the number of measurements to 18 (which is the case for the *SeaWinds* instrument system) significantly reduces the size of the high probability regions for both types of measurements. For a given direction, the wind speed determination of the 18 co-polarization measurements is very tight, but there is no directional discrimination (cf. section III). The polarimetric measurements produce much wider probable regions in speed, but there are distinctive directional gaps. By indicating ranges of directions which are unlikely, the polarimetric measurements encode information unavailable to single look set co-pol measurements. Fig. 9 shows the percentile plots for all measurements from each of the eight look sets. Each polarimetric look set encodes directional information by eliminating regions of directions which are improbable. Taken singly, the conventional co-polarization look sets provide no (or very little) directional information. As we see more clearly, in Fig. 10, the intersection of the the high probability regions from all four co-pol look sets likewise includes a large range of possible directions. The percentile plots for all co-pol measurements and all polarimetric measurements (within a given WVC) separately, and then together are shown in the left half of Fig. 10. For example WVC 1, the co-pol only case includes a large range of likely directions, a problem specific to midswath due to the unfavorable viewing geometry (i.e., azimuth diversity). The polarimetric measurements yield multiple peaks which are wide in speed, but they provide additional direction discrimination. The result of combining all co-pol and polarimetric measurements is a single peak

which is narrower in direction than the co-pol only case.

As a second example, consider a WVC located midway between nadir and the outer boundary of the swath (487.5 km away from nadir) with a wind speed of 4.88 m/s. This is the case where we have optimal viewing geometry (and thus the best performance) for the co-polarization case. The percentile plots are shown in the right half of Fig. 10. Again, the polarimetric measurements yield relatively large probable regions. The co-pol only performance is markedly different from the first example yielding sharp probability peaks. However, multiple ambiguities are present, and in fact, the highest probability peak is 171° away from the true wind direction (195°). The additional direction discrimination incorporated in the polarimetric measurements enables the selection of the correct ambiguity with high probability.

These two representative WVC's, show how wind performance can be improved despite relatively large variance in the polarimetric measurements. The dramatic directional performance improvement at midswath is due to the additional directional information available from the polarimetric measurements in a regime where the conventional co-polarization directional discrimination is often poor. Although individual polarimetric measurements may be very noisy, the variance is significantly reduced due to the large number (51) of σ_0 measurements. Furthermore, the intrinsic nature of the polarimetric model function is such that it eliminates large sets of possible directions from consideration. Even in regimes with favorable co-pol direction discrimination, the additional direction information encoded by the polarimetric measurements masks out extraneous ambiguities in the co-pol solutions, leading to significant improvements in wind direction selection skill.

C. Wind Performance Sensitivity To Polarimetric Geophysical Model Function

As stated in Section III, there are no experimental Ku-band scatterometer measurements of the polarimetric backscatter coefficients. We have assumed a PGMF constructed from the theoretical results developed in [33] and co-pol only (NSCAT) data. In order to ascertain how sensitive the simulation results are to the exact polarimetric model function, we vary the values of the PGMF parameters. We study the effect of varying two parameters: we lower the σ_{HV}/σ_{VV} ratio, which has the effect of lowering both the α_1 and α_2 terms in (5), and we reduce the up-wind/down-wind asymmetry, effectively making α_1 and α_2 more the same. In order to estimate the worst

case bounds on performance due to errors in our assumed value for either of these parameters, we simulated the following cases: (1) σ_{HV}/σ_{VV} ratio of -20 dB for all wind speeds instead of the nominal -15 dB, (2) upwind/downwind polarimetric correlation coefficient asymmetry ratio of $\delta = 0.1$ instead of $\delta = 0.5$ (see Appendix A for definition of δ) with the magnitude of the maximal case unchanged, and (3) a combination of (1) and (2). These three cases are compared with the "baseline" case in Fig. 11. Although changing the parameters causes some degradation in performance, the results are still substantially better than the nonpolarimetric case (cf. Fig. 7). Due to an ambiguity removal problem at high wind speeds nudging was required to achieve good performance in cases (2) and (3). For these two cases the upwind-downwind asymmetry of the model function is substantially degraded. Without nudging, a region of nearly 40° RMS direction error values was apparent for 10.5-30 m/s wind speeds. Nudging was not required for the other wind speed ranges. The nudged results are presented in Fig. 11 for the 10.5-30 m/s speed range for cases (2) and (3); un-nudged results were presented for all other cases and speed ranges.

D. Simulation Results Using an Enhanced Wind Retrieval Algorithm.

Scatterometer wind retrieval is an evolving area of research with many different algorithms under development. To establish that the benefits of polarimetric capability are still evident with a somewhat different algorithm than is currently implemented by the *SeaWinds* project, simulation results were computed with an advanced wind retrieval algorithm developed at JPL and currently under evaluation. The improved technique has two parts. First, during pointwise wind retrieval, probabilistic methods are used to determine error bars on the retrieved direction for each ambiguity. The standard median filtering technique is then applied for ambiguity removal. Next, the wind direction error bars that were calculated during pointwise wind retrieval, are used to improve the directional accuracy of the selected ambiguity. Information from neighboring cells is used to pick an optimum direction within the error bars. In this way, spatial information can be applied to reduce random wind direction errors without significantly degrading the resolution of the resultant wind field. For more details see [27].

Fig. 12 depicts the simulated wind performance of the baseline polarimetric and nonpolarimetric (*SeaWinds*) designs using the enhanced wind retrieval method. The performance of both

designs is improved with the enhanced technique. As before, the performance of the polarimetric design is significantly better than the nonpolarimetric performance. As with the baseline technique, nudging is not required for a PSCAT, but is required in order to obtain acceptable results with the non-polarimetric design.

VII. Summary and Conclusions

In this paper, we reviewed the wind performance of conventional wind scatterometers, which use co-polarized backscatter measurements, and discussed the limitations of such systems. A new polarimetric scatterometer concept was introduced as a technique for improving wind measurements from space. Based on a theoretical analysis, a parametric formulation for a polarimetric model function was introduced. It was shown through simulations that polarimetric measurements have great potential for improving wind speed and direction accuracy across the entire swath, as well as for alleviating the need for external wind field information in performing wind vector dealiasing. It was further shown that the introduction of polarimetric measurements is advantageous even if the magnitude of the polarimetric signature is much lower than predicted by theory. As discussed in Section IV, polarimetric capability is easily implemented with straightforward modifications to existing scatterometer systems such as *SeaWinds*.

To fully validate the assumptions and claims of this paper, airborne and, possibly, spaceborne measurement campaigns are recommended to more fully develop a polarimetric geophysical model function. The authors plan, in the near future, to conduct polarimetric ocean experiments using JPL's L- and C-band Airborne Polarimetric SAR in Monterey Bay and offshore from Santa Barbara, California to verify the functional form of the PGMF. We are also pursuing the possible implementation of polarimetric capability with the next generation of spaceborne scatterometer to be flown in the mid-2000's time frame.

Acknowledgment

The research described in this paper was carried out by the Jet Propulsion Laboratory, California Institute of Technology, under a contract with the National Aeronautics and Space Administration.

Appendix A. Calculation of Polarimetric Backscattering Coefficients

Here, we summarize the algorithm to calculate the polarimetric backscattering coefficients. From curve fitting of the azimuth modulations in the NSCAT-2 backscatter representing the azimuth anisotropy of the ocean surface, we define the factor ρ_0 by a fifth order polynomial U given by

$$\begin{aligned}\rho_0 &= 5.234187 \times 10^{-2}U - 4.635087 \times 10^{-3}U^2 + 1.5992 \times 10^{-4}U^3 \\ &\quad -2.4191 \times 10^{-6}U^4 + 1.3440 \times 10^{-8}U^5 \end{aligned} \tag{A.1}$$

where U is the neutral wind speed in m/s at 10-m height. Next, we obtain $\sigma_{VV}(U, \phi = 60°, \theta)$ from NSCAT-2 GMF at $\phi = 60°$ corresponding to the local minimum in the polarimetric correlation coefficient $\rho_{hvvv} = \sigma_{hvvv}/\sqrt{\sigma_{HV}\sigma_{VV}}$ or $\rho_{vhhh} = \sigma_{vhhh}/\sqrt{\sigma_{HV}\sigma_{HH}}$ to determine the scale factor $\alpha(U, \theta)$

$$\alpha(U, \theta) = \frac{\sqrt{e_V}\rho(U, \theta)\sigma_{VV}(U, \phi = 60°, \theta)}{(1 + \delta)\sin(120°) - \delta\sin(60°)} \tag{A.2}$$

In (8), $\rho(U, \theta) = 0.5\rho_0(1 + \theta/30)$ with θ given in degrees and δ is a factor representing the upwind and downwind asymmetry. To calculate the polarimetric backscattering coefficient σ_{hvvv} given by (5). We specify coefficient $\alpha_1(U, \theta, hvvv)$ and $\alpha_2(U, \theta, hvvv)$

$$\begin{aligned}\alpha_1(U, \theta, hvvv) &= -\xi\delta\alpha(U, \theta) \\ \alpha_2(U, \theta, hvvv) &= \xi(1 + \delta)\alpha(U, \theta) \end{aligned} \tag{A.3}$$

where ξ is the signal attenuation. To match with the theoretical calculated ρ_{hvvv} at the moderate wind, we set $\xi = 1$ and $\delta = 0.5$. Then it is straight forward to compute σ_{hvvv} according to (5). To calculate the polarimetric backscattering coefficient $\sigma_{vhhh} = \rho_{vhhh}\sqrt{e_V\sigma_{VV}\sigma_{HH}}$, we use $|\rho_{vhhh}| = |\rho_{hvvv}|$ and $\angle\rho_{vhhh} = -\angle\rho_{hvvv}$ with σ_{VV} and σ_{HH} determined by NSCAT-2 GMF.

Note that the above PGMF is an estimate given the lack of experimental data and uncertainties in the hydrodynamic model for the surface roughness spectrum as well as approximations in the electromagnetic scattering model. Furthermore, scattering from ocean surface, even for the co-polarization backscatter, is not well understood at low and high winds where ocean backscatter needs further investigation [2, 4, 21]. In view of the uncertainties, we have built in the above formulation of the PGMF several factors such as the cross-polarization ratio e_V, the asymmetry

factor δ, and the signal attenuation ξ. These factors can be changed to modify the characteristics of the polarimetric signatures, to study their effects, and to investigate their sensitivities or robustness in the simulation of the polarimetric scatterometer system for wind vector retrieval.

References

[1] E.P.W. Attema, "The Active Microwave Instrument On-Board the ERS-1 Satellite," *Proceedings of the IEEE*, Vol. 79, No. 6, pp. 791-799, June 1991.

[2] J. R. Carswell, S. C. Carson, R. E. McIntosh, F. K. Li, G. Neumann, D. J. McLaughlin, J. C. Wilkerson, P. G. Black, and S. V. Nghiem, "Airborne scatterometers: Investigating ocean backscatter under low- and high-wind conditions," *Proceedings of the IEEE*, vol. 82, no. 12, pp. 1835-1860, 1994.

[3] C-Y Chi, R. Aroian, F. K. Li, "Simulation Studies for the NASA Scatterometer on NROSS," *Proceedings of IGARSS'86*, Zurich, September 1986, pp. 1673-1676.

[4] M. A. Donelan and W. J. Pierson, "Radar scattering and equilibrium ranges in wind-generated waves with application to scatterometry," *J. Geophys. Res.*, vol. 92, no. C5, pp. 4971-5029, 1987.

[5] R. S. Dunbar, "NASA scatterometer science data product (NSCAT-2) User's Manual - overview and geophysical data products," JPL Document, D-12985 Manual Version 1.2, February 1998.

[6] R. Fisher, "Standard Deviation of Scatterometer Measurements From Space," *IEEE Trans. Geosci. Electron.*, Vol. GE-10, No. 2, April 1972.

[7] Freilich, M. H., and R. S. Dunbar (1993). "A Preliminary C-Band Scatterometer Model Function for the ERS-1 AMI Instrument", Proc. of the First ERS-1 Symposium, ESA SP-359, pp. 79-84.

[8] Freilich, M. H., H. Qi, and R. S. Dunbar, 1998, "A Ku-band scatterometer model function from NSCAT measurements and operational global surface wind analyses," J. Geophys. Res. (in prep.).

[9] J. Graf, W. Tsai, and L. Jones, "Overview of QuikSCAT Mission - a quick deployment of a high resolution, wide swath scanning scatterometer for ocean measurement," Proc. Southeast AGU conference, April 1998, Orlando, Florida.

[10] W. L. Grantham, E. M. Bracalente, W. L. Jones, and J. W. Johnson, "The Seasat-A satellite scatterometer," IEEE J. Oceanic Eng., Vol OE-2, pp 200-206, 1977

[11] S. Haykin, *Communication Systems*, 2nd ed., New York: Wiley, 1983.

[12] J. Huddleston, W. Tsai, M. Spencer, R. West, "Modeling and Simulation for SeaWinds-1B System Design and Performance Evaluation," EOS/SPIE Aerospace Remote Sensing Journal, London, England, September 1997].

[13] W. L. Jones, et. al., "The Seasat-A satellite scatterometer: the geophysical evaluation remote sensed winds over the ocean," J. Geophys. Res., Vol 87, pp 3297-3317, 1982

[14] P. Lecompte, "The ERS Scatterometer Instrument and the On-Ground Processing of its Data," in Emerging Scatterometer Applications: From Research to Operations, ESA Publication SP-424.

[15] Proceedings of the NASA Scatterometer Science Symposium, 10-14 November 1997, Maui, Hawaii, USA, Timothy Liu, editor.

[16] D.G. Long and M.W. Spencer, "Radar Backscatter Measurement Accuracy for a Spaceborne Pencil-Beam Wind Scatterometer with Transmit Modulation," *IEEE Transactions on Geoscience and Remote Sensing*, Vol 35, No. 1, pp. 102-114, Jan. 1997.

[17] R.K. Moore and A.K. Fung, "Radar Determination of Winds at Sea," *Proceedings of the IEEE*, Vol. 67, No. 11, November, 1997, pp. 1504-1521.

[18] F. M. Naderi, M. H. Freilich, D. G. Long, "Spaceborne Radar Measurement of Wind Velocity Over the Ocean - An Overview of the NSCAT Scatterometer System," Proc. of the IEEE, vol. 79, no. 6, pp. 850-866, June 1991

[19] S. V. Nghiem, M. Borgeaud, J. A. Kong, and R. T. Shin, "Polarimetric remote sensing of geophysical media with layer random medium model," *Progress in Electromagnetics Research*, ed. J. A. Kong, Vol. 3, Chap. 1, pp. 1-73, Elsevier, New York, 1990.

[20] S. V. Nghiem, S. H. Yueh, R. Kwok, and F. K. Li, "Symmetry properties in polarimetric remote sensing," *Radio Sci.*, vol. 27, no. 5, pp. 693-711, 1992.

[21] S. V. Nghiem, F. K. Li, S. H. Lou, G. Neumann, R. E. McIntosh, S. C. Carson, J. R. Carswell, E. J. Walsh, M. A. Donelan, W. M. Drennan, "Observations of ocean radar backscatter at Ku and C bands in the presence of large waves during the Surface Wave Dynamics Experiment," *IEEE Trans. Geosci. Remote Sens.*, vol. 33, no. 3, pp. 708-721, 1995.

[22] S. V. Nghiem, F. K. Li, and G. Neumann, "The dependence of ocean backscatter at K_u-Band on oceanic and atmospheric parameters," *IEEE Trans. Geosci. Remote Sens.*, vol. 35, no. 3, pp. 581-600, 1997.

[23] L. C. Schroeder, P. R. Schaffner, J. L. Mitchell, and W. L. Jones, "AAFE RADSCAT 13.9-GHz measurements and analysis: Wind-speed signature of the ocean," *IEEE J. Oceanic Engineering*, vol. OE-10, no. 4, pp. 346-357, 1985.

[24] S.J. Shaffer, R.S. Dunbar, S.V. Hsiao, and D.G. Long, "A median-filter-based ambiguity removal algorithm for NSCAT," IEEE Transactions on Geoscience and Remote Sensing, Vol 29, No. 1, pp. 167-174, Jan., 1991.

[25] M.W. Spencer, C. Wu, and D.G. Long, "Tradeoffs in the Design of a Spaceborne Scanning Pencil Beam Scatterometer: Application to SeaWinds," IEEE Transactions on Geoscience and Remote Sensing, Vol 35, No. 1, pp. 115-126, Jan., 1997.

[26] M.W. Spencer, C. Wu, and D.G. Long, "Improved Resolution Backscatter Measurements with the *SeaWinds* Pencil-Beam Scatterometer," submitted to *IEEE Trans. Geosci. Remote Sensing*, 1998.

[27] B. Stiles and B. Pollard, "A probabilistic approach to nadir performance enhancement for pencil beam scatterometers," Jet Propulsion Laboratory Document no. D-17029.

[28] F. J. Wentz, S. Peteherych, and L. A. Thomas, "A model function for ocean radar cross sections at 14.6 GHz," *J. Geophys. Res.*, vol. 89, no. C3, pp. 3689-3704, 1984.

[29] F. J. Wentz, L. A. Mattox, and S. Peteherych, "New algorithms for microwave measurements of ocean winds: Applications to SEASAT and the Special Sensor Microwave Imager," *J. Geophys. Res.*, vol. 91, no. C2, pp. 2289-2307, 1986.

[30] Wentz, F. J. and D. K. Smith, "A model function for the ocean normalized cross section at 14 GHz derived from NSCAT observations," J. Geophys. Res. (submitted).

[31] R. West, "SeaWinds on QuikSCAT Scanning Pencil-Beam Scatterometer Simulator," JPL Report D-17309, May 1999.

[32] C. Wu, J. Graf, M. Freilich, D. G. Long, M. Spencer, W. Tsai, D. Lisman, and C. Winn, "The SeaWinds scatterometer instrument," IGARSS '94 Proc., pp 1511-1515, August 1994

[33] S.H. Yueh, R. Kwok, S.V. Nghiem, "Polarimetric Scattering and Emission Properties of Targets With Reflection Symmetry," *Radio Science*, Vol. 29, Number 6, pp. 1409-1420, Nov-Dec 1994.

[34] S. H. Yueh, W. J. Wilson, F. K. Li, W. B. Ricketts, and S. V. Nghiem, "Polarimetric measurements of sea surface brightness temperatures using an aircraft K-band radiometers," IEEE Trans. Geosci. Remote Sensing, Vol 33, pp 85-92, 1995

[35] S. H. Yueh, W. J. Wilson, F. K. Li, W. B. Ricketts, and S. V. Nghiem, "Polarimetric brightness temperatures of sea surfaces measured with aircraft Ku- and Ka-band radiometers," IEEE Trans. Geosci. Remote Sensing, Vol 35, No. 5, 1997

Captions

Table 1: Key *SeaWinds* instrument system parameters.

Figure 1: (a) *SeaWinds* scanning and measurement geometry for the inner and outer beams. (b) Figure showing how the backscatter cross-section over a given wind vector cell on the ocean surface is measured at four times at four different azimuth angles.

Figure 2: NUSCAT co-pol and cross-pol measurements for 2.9 to 3.5 m/s wind speed, showing that the cross-polarization ration (σ_{HV}/σ_{VV}) is on the order of -15 dB.

Figure 3: Plots of co-polarization and polarimetric geophysical model functions for (a) σ_{VV} at 54° incidence, (b) σ_{HH} at 46° incidence, (c) σ_{hvvv} at 54° incidence, and (d) σ_{vhhh} at 46° incidence.

Figure 4: Sample plots of "noise-free" retrieved wind vector solutions from multiple σ_0 measurements at a given wind vector cell for (a) a one-beam co-pol system, (b) a two-beam co-pol systems, and (c) a two-beam system with both co-pol and polarimetric capability.

Figure 5: (a) Functional block diagram for current *SeaWinds* scatterometer systems to be flown on *QuikSCAT* and ADEOS-2. (b) Modifications required for adding polarimetric capability.

Figure 6: Functional block diagram for *SeaWinds* end-to-end simulator.

Figure 7: Comparison of baseline polarimetric and conventional scatterometer (SeaWinds) wind direction and speed errors. Figure 7a: depicts the RMS wind direction error of the selected ambiguities for both systems as a function of cross track distance. Figure 7b: depicts the RMS wind speed error.

Figure 8: Percentile plots for polarimetric and co-pol inner beam forward looking σ_0 measurements. (Example Wind Vector Cell 1) Dark region denote areas of high probability. The dashed line encloses 80% probable regions. Plots are presented for single co-pol and polarimetric measurements and for all 18 measurements of each type. Individual polarimetric measurements provide little information, but when all 18 are considered they provide direction discrimination unavailable to co-polarization measurements from a single look geometry.

Figure 9: Percentile plots for polarimetric and co-pol σ_0 measurements from all four look geometries. (Example Wind Vector Cell 1) Distinctive directional gaps occur in the high probability regions for the polarimetric look sets, so that when all four look sets are combined a significant amount of directional discrimination is available.

Figure 10: Percentile plots for all polarimetric, all co-pol σ_0 measurements, and the two sets combined. The high probability regions in the combined case are roughly equal to the intersections of those from the polarimetric and co-pol cases. The three plots on the left are for a wind vector cell at midswath a regime in which poor co-pol only directional discrimination is aided by polarimetric measurements. The three plots on the right are for a swath region in which the co-pol directional discrimination is better, but the polarimetric information is still useful for eliminating extraneous ambiguities.

Figure 11: PSCAT Performance Sensitivity to PGMF Parameters. The baseline (thick solid line) case is compared to cases with lower cross-pol ratio (thin dotted line), less upwind-downwind

asymmetry (thick dashed line) and the two cases combined (thin solid line). Figure 11a: depicts the RMS wind direction error of the selected ambiguities for all for cases as a function of cross track distance. Figure 11b: depicts the RMS wind speed error.

Figure 12: Comparison of polarimetric and conventional scatterometer (SeaWinds) performance using enhanced wind retrieval algorithm. Figure 12a: depicts the RMS wind direction error of the selected ambiguities for both systems as a function of cross track distance. Figure 12b: depicts the RMS wind speed error.

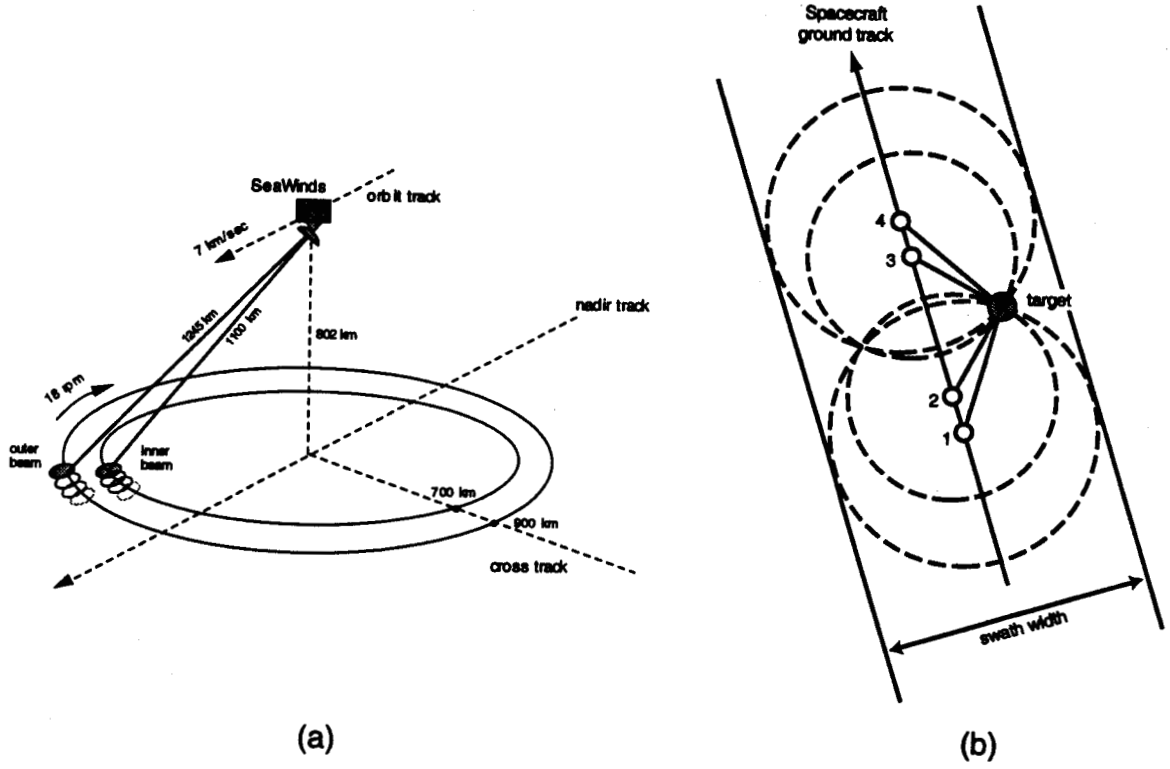
SeaWinds
orbit track
7 km/sec
1245 km
1100 km
802 km
nadir track
18 rpm
outer beam
inner beam
700 km
900 km
cross track
(a)
Spacecraft ground track
4
3
target
2
1
swath width
(b)

Figure 1:

Figure 2:

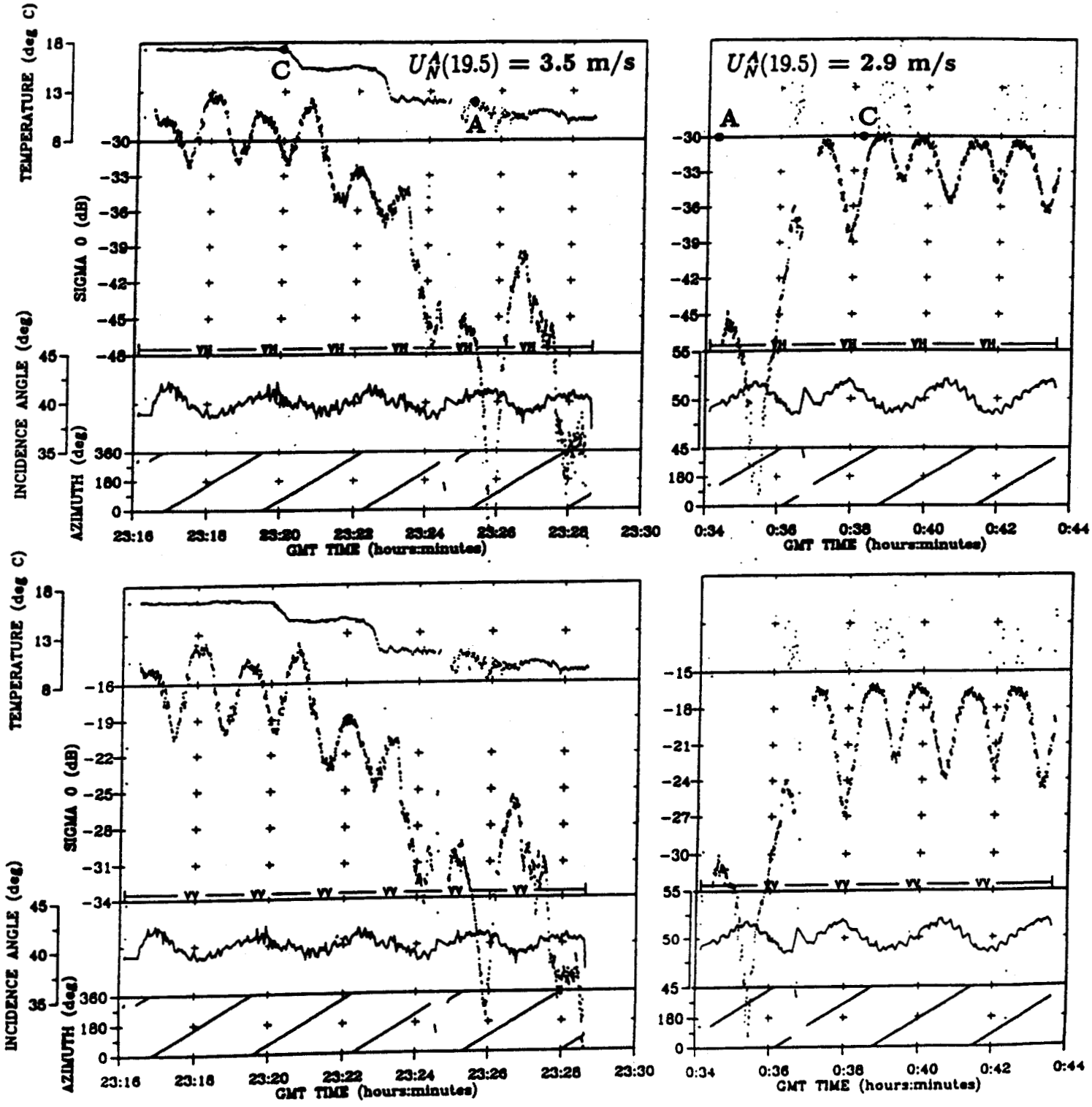
$U_N^A(19.5) = 3.5$ m/s
$U_N^A(19.5) = 2.9$ m/s
TEMPERATURE (deg C)
SIGMA 0 (dB)
INCIDENCE ANGLE (deg)
AZIMUTH (deg)
GMT TIME (hours:minutes)
VH
VV
A
C

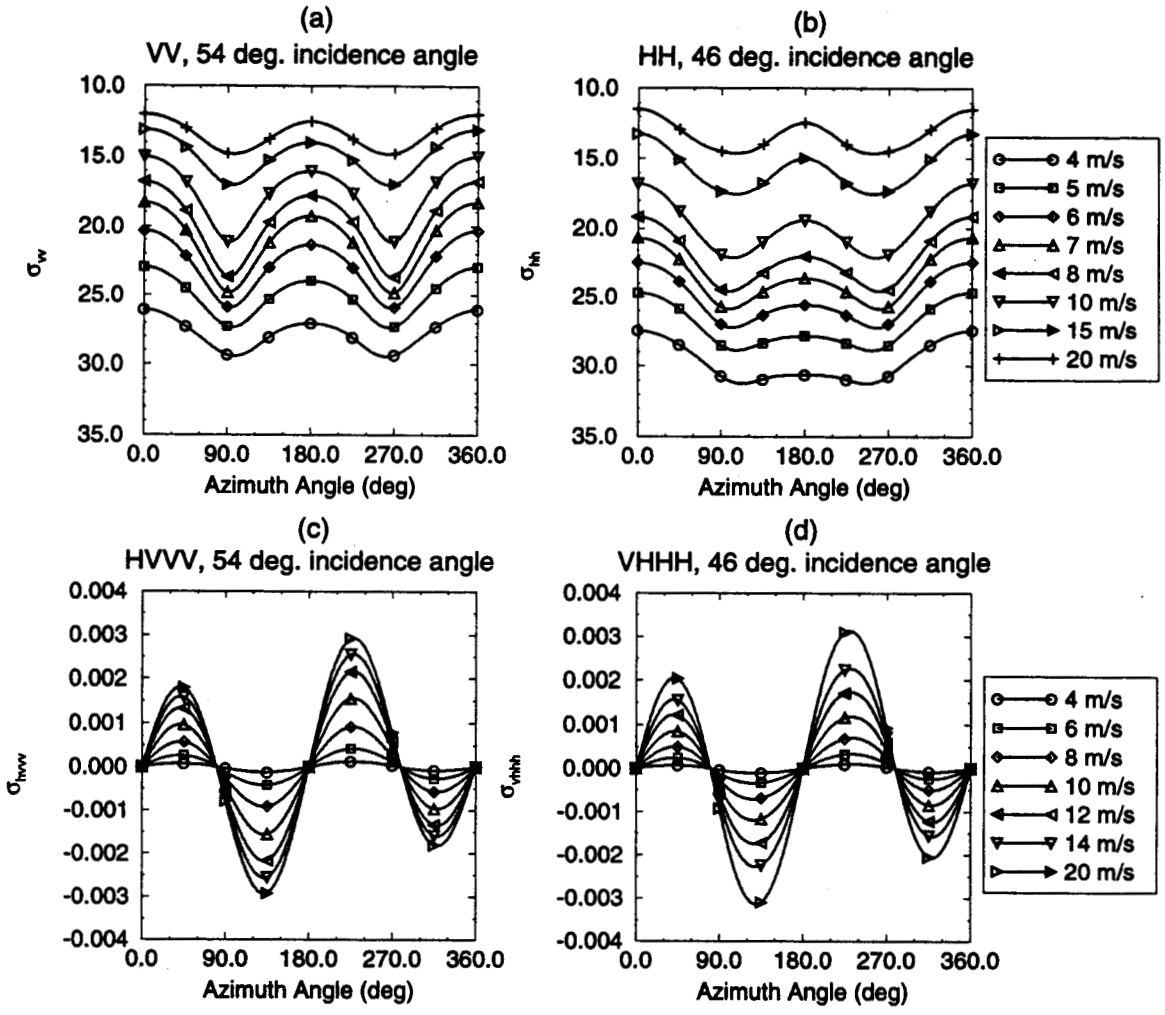
(a)
VV, 54 deg. incidence angle
σ_{vv}
10.0
15.0
20.0
25.0
30.0
35.0
0.0
90.0
180.0
270.0
360.0
Azimuth Angle (deg)
(b)
HH, 46 deg. incidence angle
σ_{hh}
4 m/s
5 m/s
6 m/s
7 m/s
8 m/s
10 m/s
15 m/s
20 m/s
(c)
HVVV, 54 deg. incidence angle
σ_{hvv}
0.004
0.003
0.002
0.001
0.000
-0.001
-0.002
-0.003
-0.004
(d)
VHHH, 46 deg. incidence angle
σ_{vhh}
4 m/s
6 m/s
8 m/s
10 m/s
12 m/s
14 m/s
20 m/s

Figure 3:

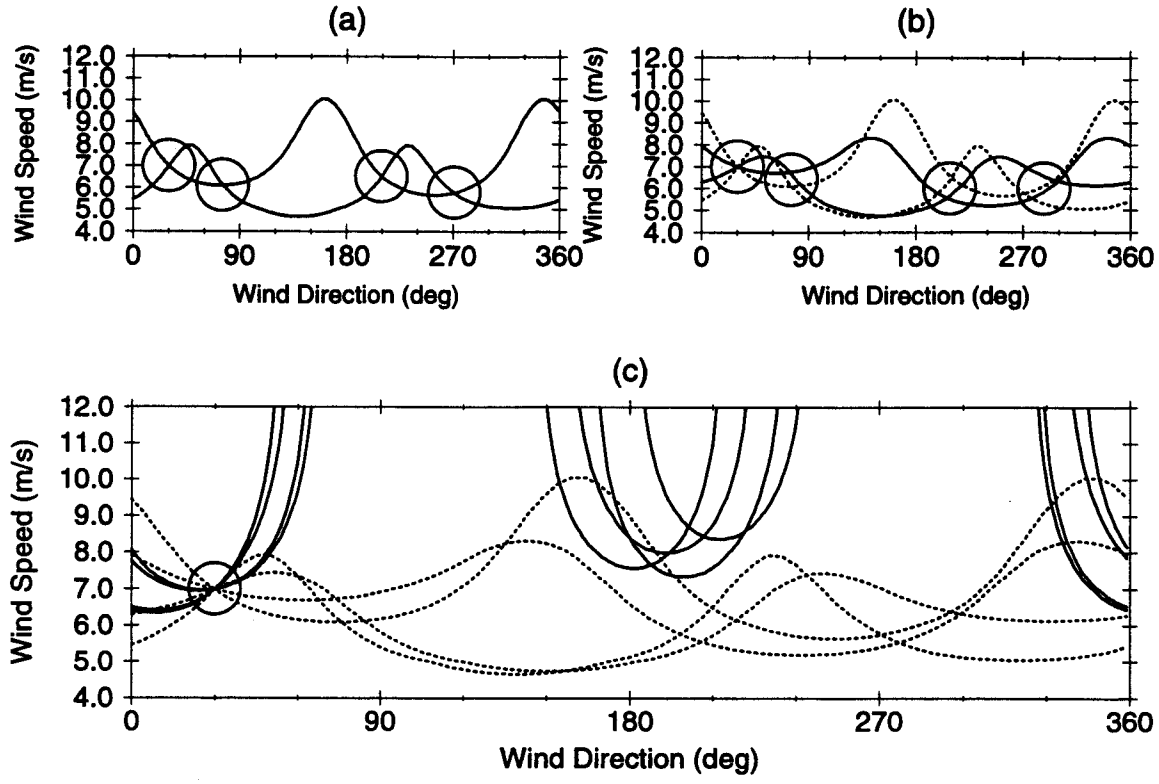
(a)
(b)
(c)
Wind Speed (m/s)
Wind Direction (deg)
12.0
11.0
10.0
9.0
8.0
7.0
6.0
5.0
4.0
0
90
180
270
360

Figure 4:

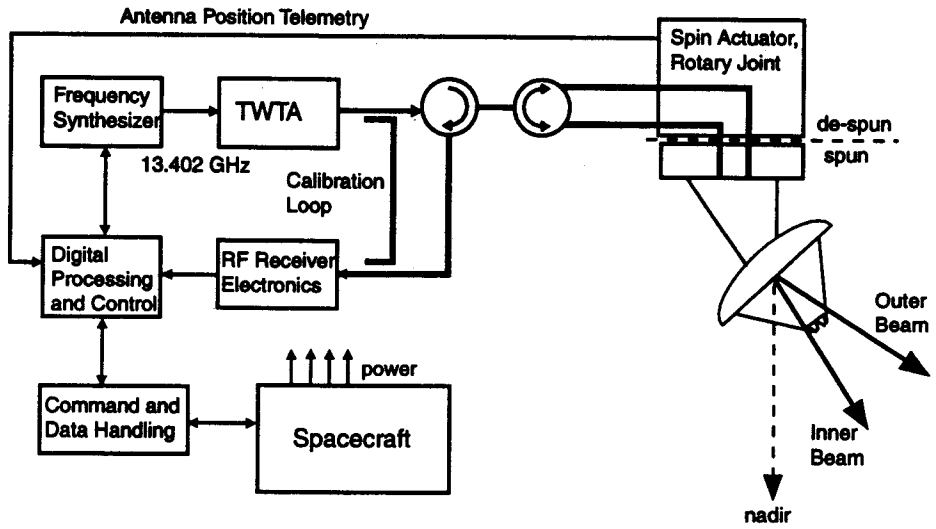
Antenna Position Telemetry
Spin Actuator, Rotary Joint
Frequency Synthesizer
TWTA
13.402 GHz
Calibration Loop
de-spun
spun
Digital Processing and Control
RF Receiver Electronics
Outer Beam
power
Command and Data Handling
Spacecraft
Inner Beam
nadir

(a)

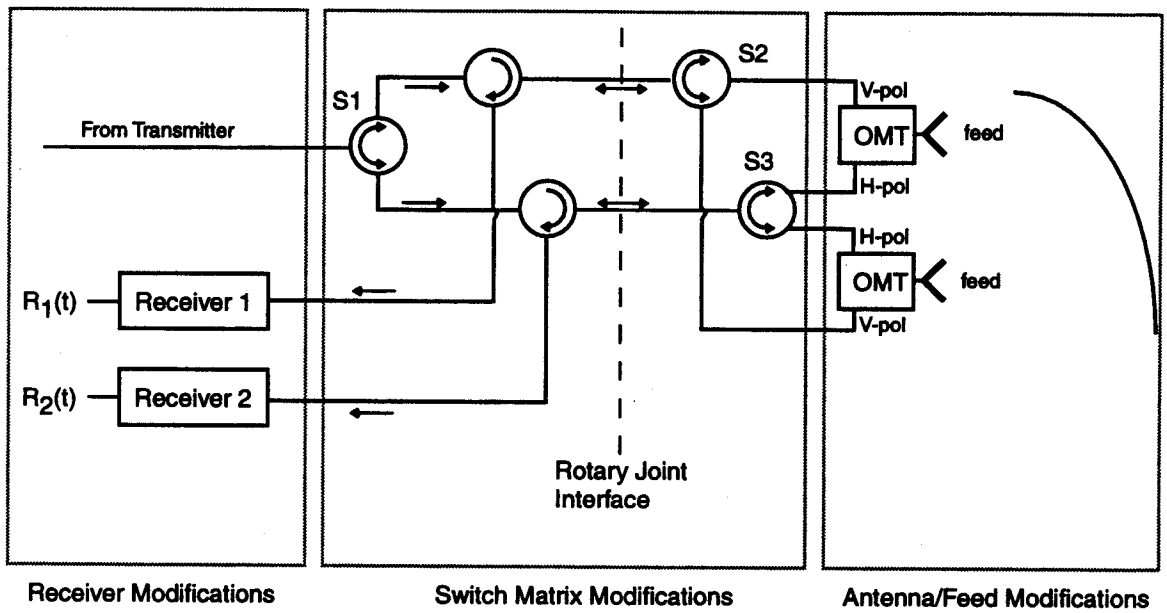
S1
S2
S3
From Transmitter
V-pol
OMT
feed
H-pol
H-pol
OMT
feed
V-pol
R1(t)
Receiver 1
R2(t)
Receiver 2
Rotary Joint Interface
Receiver Modifications
Switch Matrix Modifications
Antenna/Feed Modifications

(b)

Figure 5:

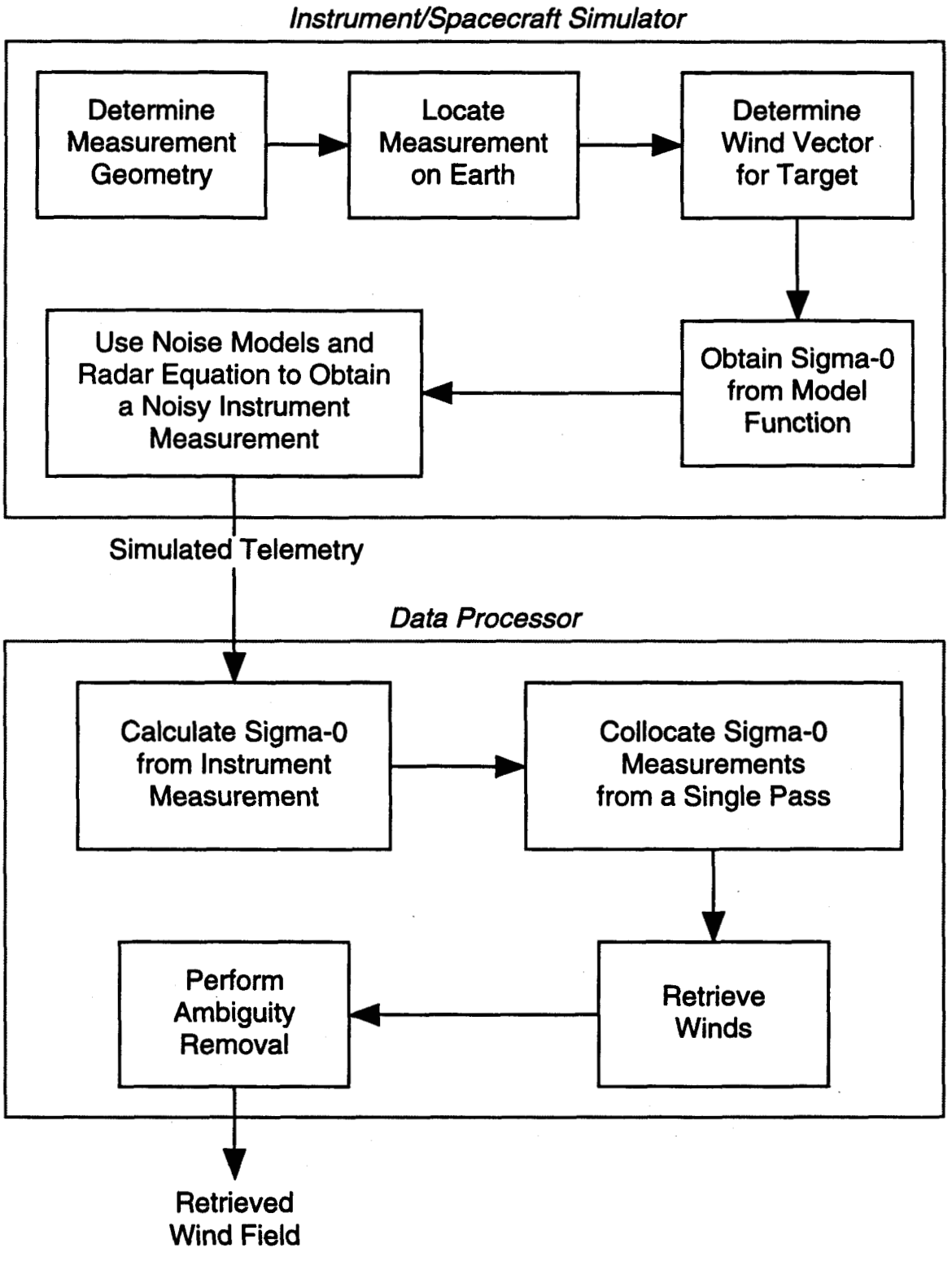
Instrument/Spacecraft Simulator
Determine Measurement Geometry
Locate Measurement on Earth
Determine Wind Vector for Target
Obtain Sigma-0 from Model Function
Use Noise Models and Radar Equation to Obtain a Noisy Instrument Measurement
Simulated Telemetry
Data Processor
Calculate Sigma-0 from Instrument Measurement
Collocate Sigma-0 Measurements from a Single Pass
Retrieve Winds
Perform Ambiguity Removal
Retrieved Wind Field

Figure 6:

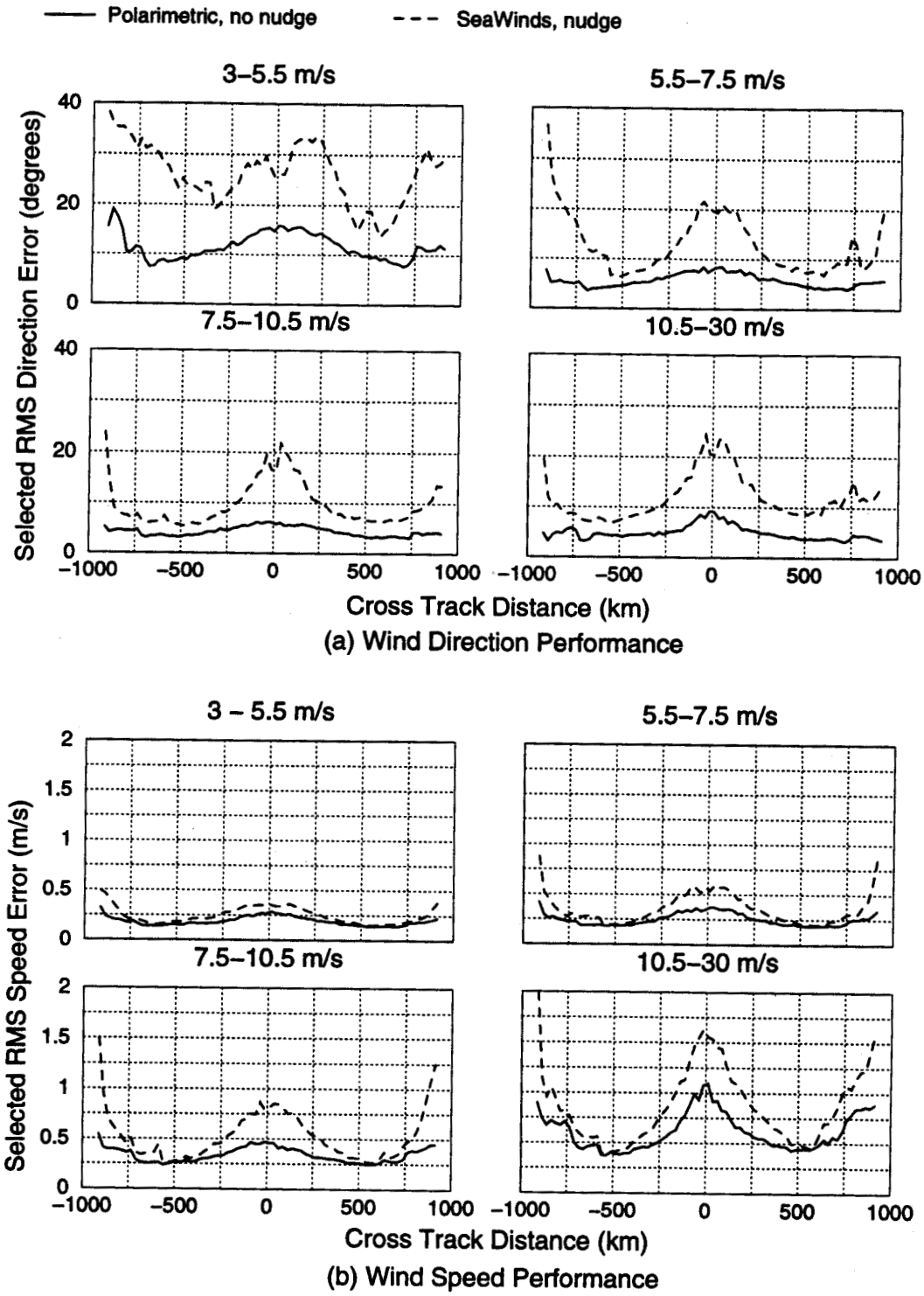
Polarimetric, no nudge
SeaWinds, nudge
3–5.5 m/s
5.5–7.5 m/s
7.5–10.5 m/s
10.5–30 m/s
Selected RMS Direction Error (degrees)
40
20
0
−1000
−500
0
500
1000
Cross Track Distance (km)
(a) Wind Direction Performance
3 – 5.5 m/s
5.5–7.5 m/s
7.5–10.5 m/s
10.5–30 m/s
Selected RMS Speed Error (m/s)
2
1.5
1
0.5
0
−1000
−500
0
500
1000
Cross Track Distance (km)
(b) Wind Speed Performance

Figure 7:

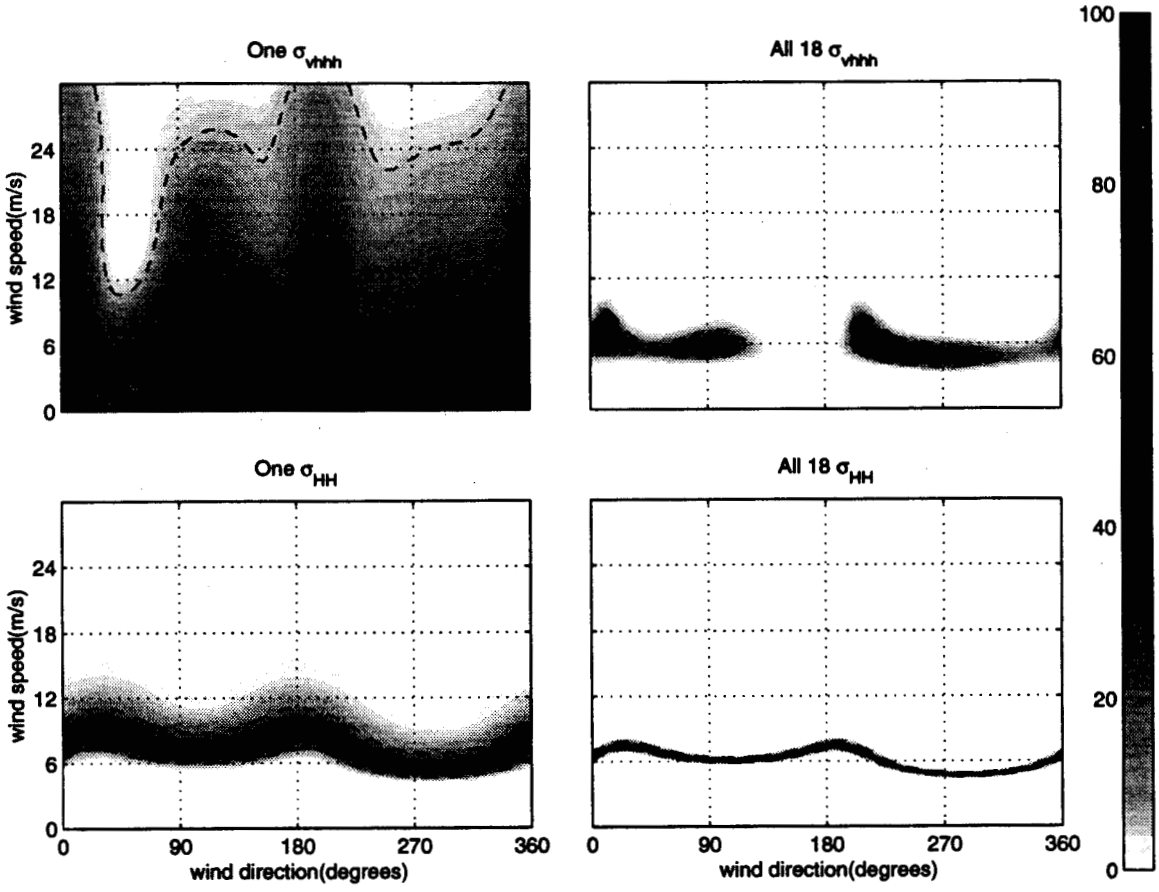
One σ_{vhhh}
All 18 σ_{vhhh}
One σ_{HH}
All 18 σ_{HH}
wind speed(m/s)
0
6
12
18
24
wind direction(degrees)
0
90
180
270
360
100
80
60
40
20
0

Figure 8:

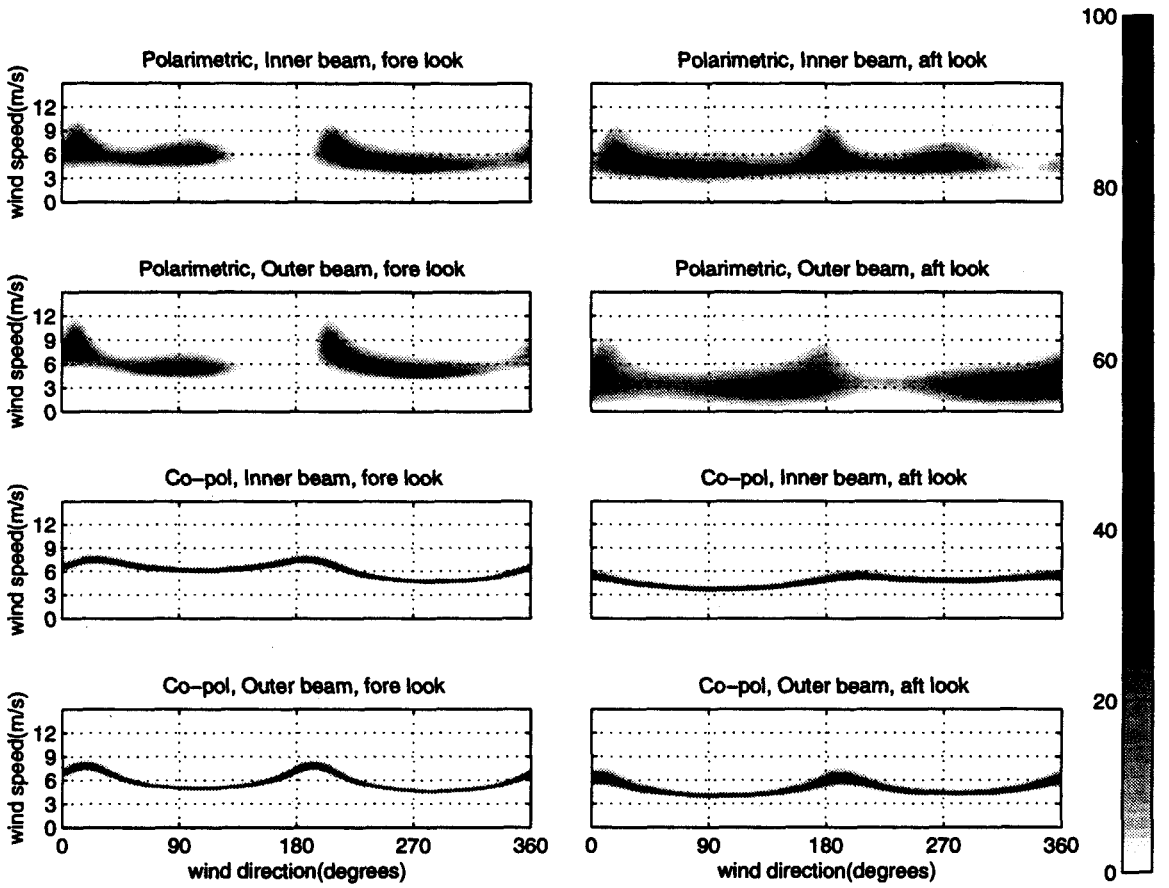
Polarimetric, Inner beam, fore look
Polarimetric, Inner beam, aft look
Polarimetric, Outer beam, fore look
Polarimetric, Outer beam, aft look
Co–pol, Inner beam, fore look
Co–pol, Inner beam, aft look
Co–pol, Outer beam, fore look
Co–pol, Outer beam, aft look
wind speed(m/s)
0
3
6
9
12
0
90
180
270
360
wind direction(degrees)
100
80
60
40
20
0

Figure 9:

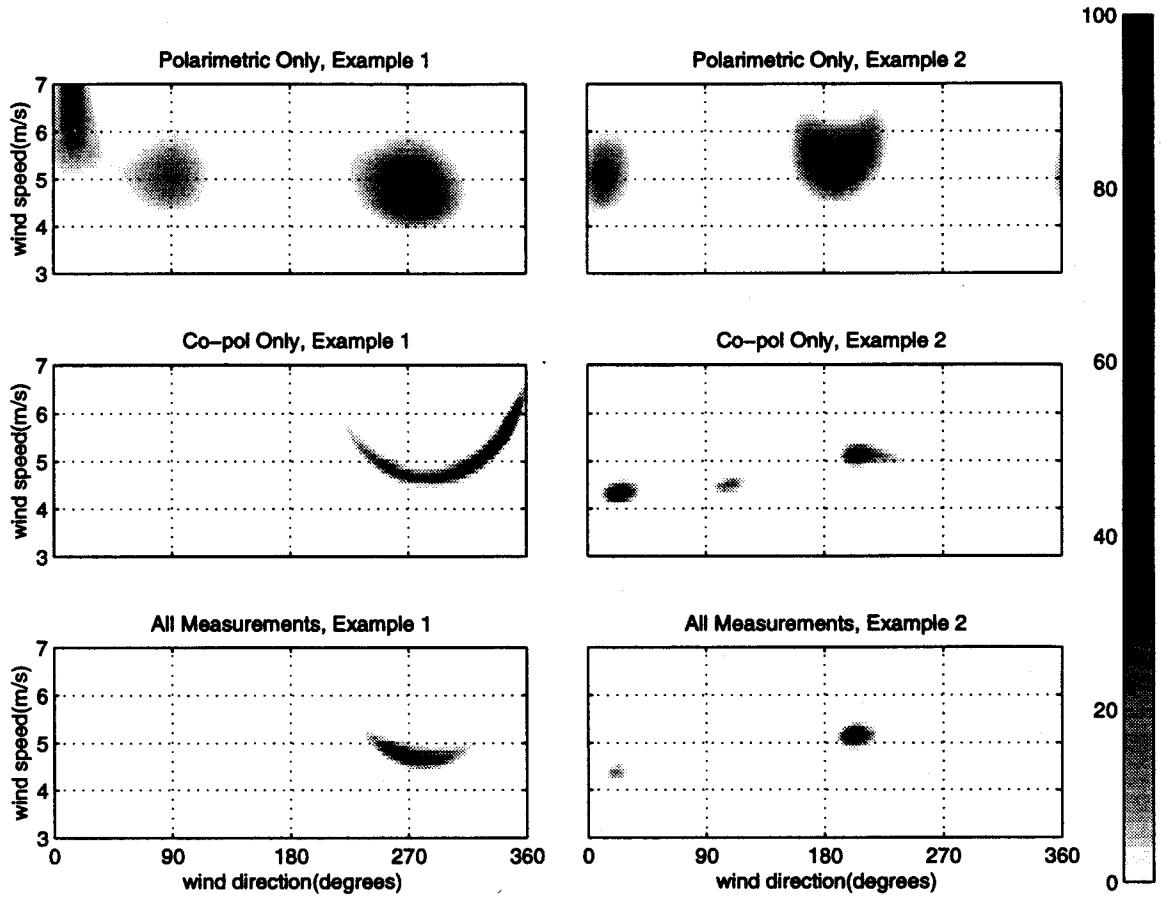
Polarimetric Only, Example 1
Polarimetric Only, Example 2
Co-pol Only, Example 1
Co-pol Only, Example 2
All Measurements, Example 1
All Measurements, Example 2
wind speed(m/s)
wind direction(degrees)
0
90
180
270
360
3
4
5
6
7
100
80
60
40
20
0

Figure 10:

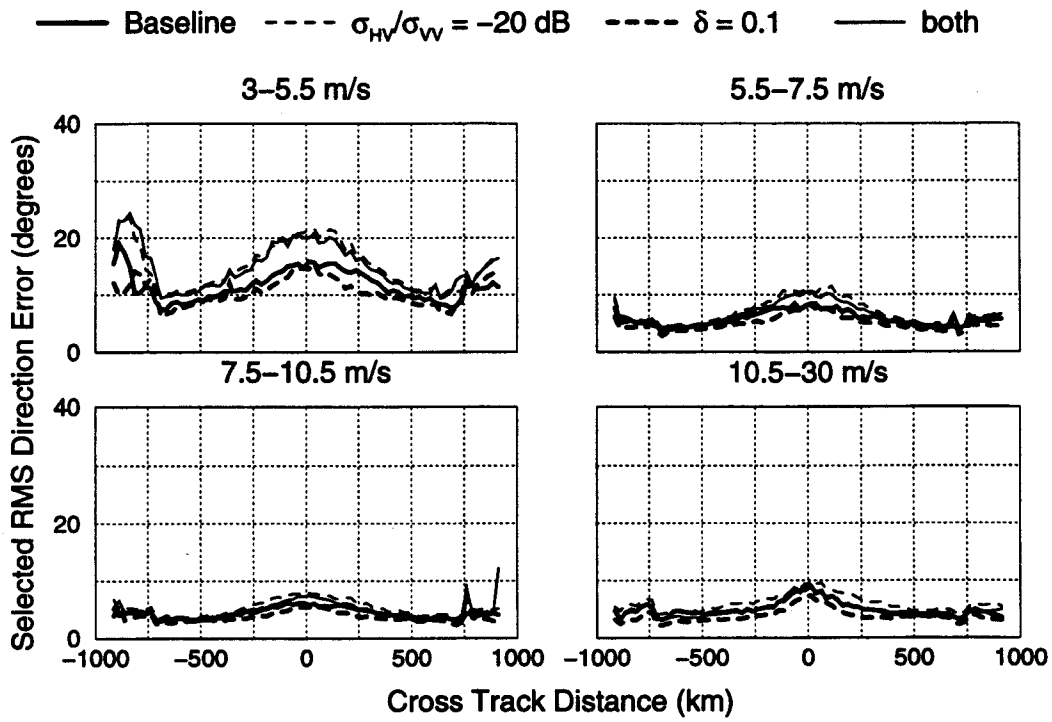

(a) Wind Direction Performance

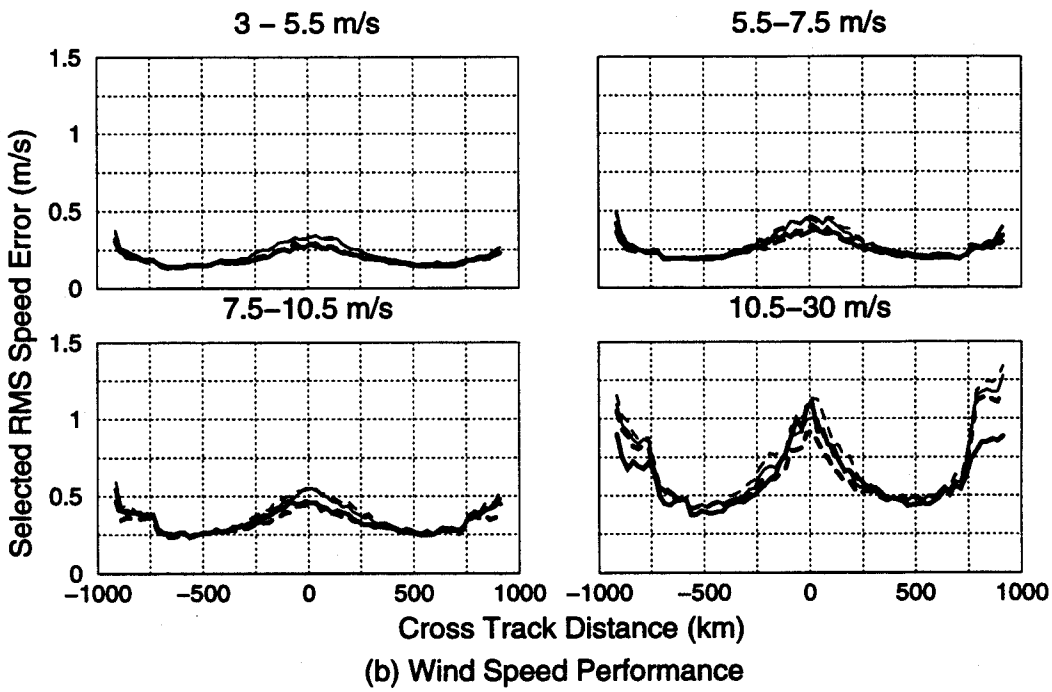

(b) Wind Speed Performance

Figure 11:

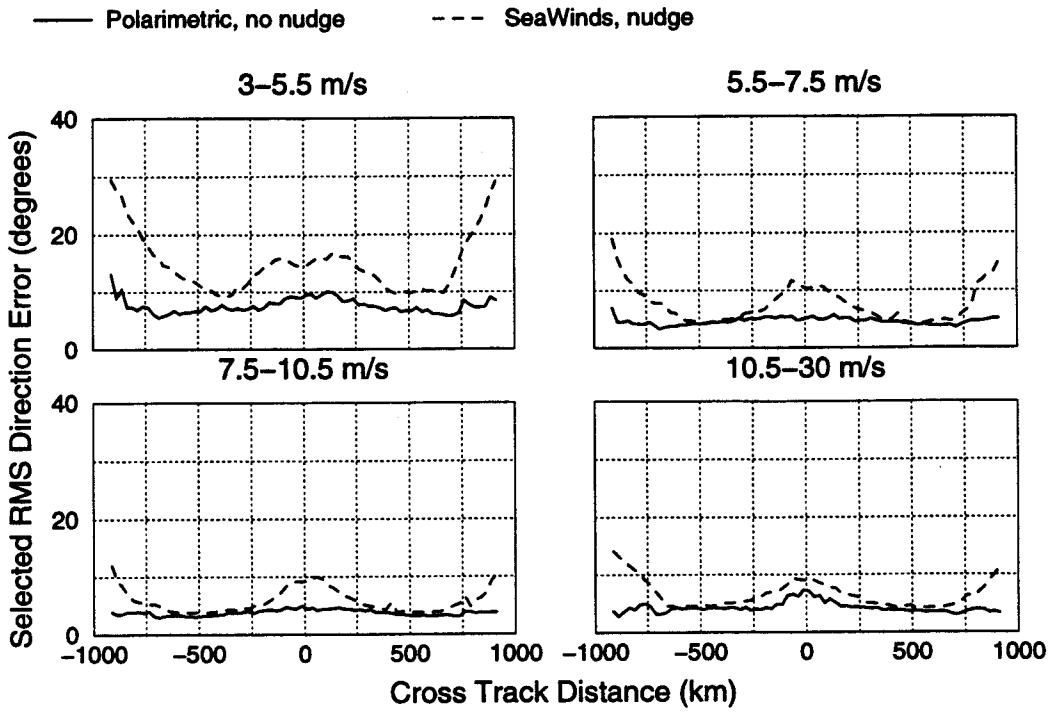

(a) Wind Direction Performance — Enhanced Technique

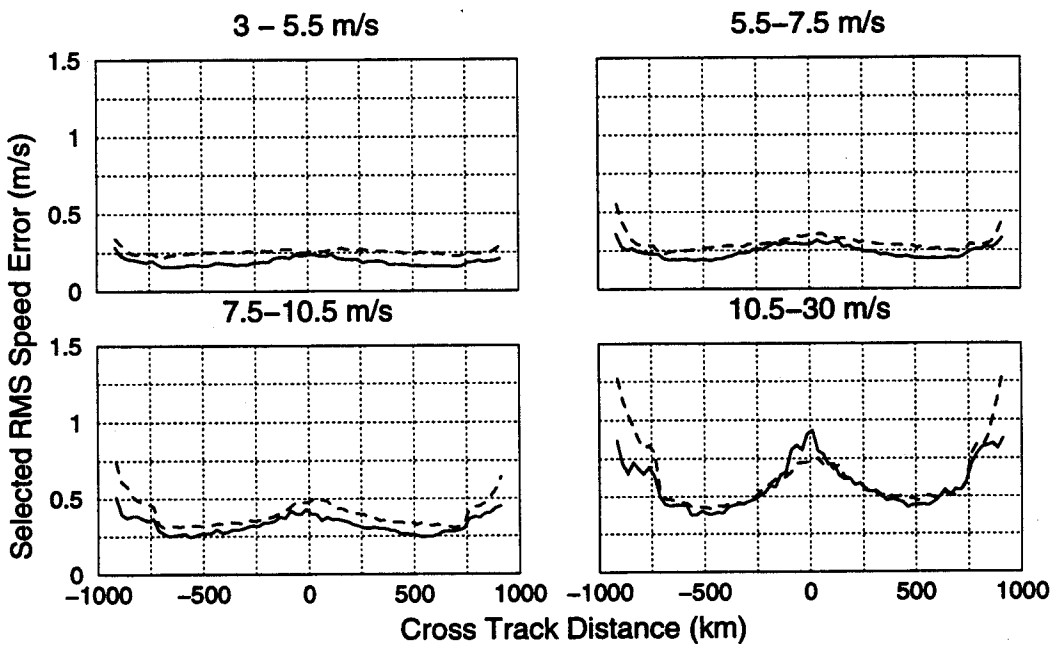

(b) Wind Speed Performance — Enhanced Technique

Figure 12: